Geochemical and textural investigations of the Eoarchean Ukaliq supracrustals, Northern Québec (Canada)

Wriju Chowdhury, Dustin Trail, Martin Guitreau, Elizabeth Bell, Jacob Buettner, Stephen Mojzsis

▶ **To cite this version:**

Wriju Chowdhury, Dustin Trail, Martin Guitreau, Elizabeth Bell, Jacob Buettner, et al.. Geochemical and textural investigations of the Eoarchean Ukaliq supracrustals, Northern Québec (Canada). Lithos, 2020, 372-373, pp.105673. 10.1016/j.lithos.2020.105673 . hal-03101296

HAL Id: hal-03101296

https://uca.hal.science/hal-03101296

Submitted on 11 Jan 2021

Geochemical and textural investigations of the Eoarchean Ukaliq Supracrustals, Northern Québec (Canada)

Wriju Chowdhury[1], Dustin Trail[1], Martin Guitreau[2],

Elizabeth A. Bell[3], Jacob Buettner[1] & Stephen J. Mojzsis[4,5]

[1] Department of Earth & Environmental Sciences, University of Rochester, Rochester, NY 14627, USA.

[2] Université Clermont Auvergne, Laboratoire Magmas et Volcans, F-63000 Clermont-Ferrand, France

[3] Earth, Planetary and Space Sciences, University of California, Los Angeles, 595 Charles Young Drive East, Box 951567, Los Angeles, CA 90095-1567, USA.

[4] Department of Geological Sciences, University of Colorado, UCB 399, 2200 Colorado Avenue, Boulder, Colorado 80309-0399, USA

[5] Hungarian Academy of Sciences, Budapest, Hungary

Corresponding author: Wriju Chowdhury (wchowdhu@ur.rochester.edu)

Keywords: Inukjuak domain, Ukaliq Supracrustal Belt, Eoarchean, zircon, thin section images, Silicon isotopes, U-Pb geochronology and Lu-Hf isotopes.

Structural, geochronological and geochemical studies of pre-3.75 Ga rocks of volcano-sedimentary protoliths in the Inukjuak domain in the Superior Province in Québec have been mostly focused on the Nuvvuagittuq Supracrustal Belt (NSB). The Porpoise Cove outcrops – at the southwestern limit of the NSB – are the *de-facto* “type locality” for the supracrustals of the Inukjuak Complex. Yet, it remains unclear whether the NSB rocks are geochemically distinct from, or are in fact common to, a host of other supracrustal enclaves locked in the dominantly gneissic Inukjuak domain. Here, we report detailed textural and geochemical studies for a suite of rocks from the Ukaliq Supracrustal Belt (USB), located approximately 3 km northeast of the NSB. We find that the USB and NSB have a similar protracted metamorphic history; both experienced amphibolite grade metamorphism and contain granitoid gneiss sheets, quartz-magnetite rocks (banded iron-formation *s.l.*) and quartz-biotite schists within amphibolitized rocks of basaltic affinity with local retrogressions. If the various Inukjuak supracrustal belts were once a part of a larger coherent (now dismembered) terrane, they should show similar emplacement ages and source chemistry. New zircon U-Pb geochronology from five gneissic units and two quartz-biotite (metasedimentary) schists reveal the oldest emplacement ages across all units of each individual rock type to be 3.68 ± 0.07 Ga (granitoid gneisses) and 3.65 ± 0.06 Ga (quartz-biotite). These new ages are similar to those documented as likely minimum emplacement ages of the NSB determined by U-Pb geochronology. Zircons from the quartz-biotite schist were also analyzed by ion microprobe U-Pb geochronology and were found to yield statistically identical, albeit more precise, ages than those obtained by LA-ICP-MS. Possible detrital zircons from the USB quartz-biotite schists were analyzed by ion microprobe for their coupled $\delta^{30}\mathrm{Si}_{\mathrm{NBS28}}$ and $\delta^{18}\mathrm{O}_{\mathrm{VSMOW}}$ values with respective values between -0.75 and -0.07 ‰ ($\delta^{30}\mathrm{Si}_{\mathrm{NBS28}}$), and +5.61 and +6.59 ‰ ($\delta^{18}\mathrm{O}_{\mathrm{VSMOW}}$). The $\delta^{18}\mathrm{O}_{\mathrm{VSMOW}}$ values, which are on average above mantle-derived zircon, indicate contribution of altered, non-mantle derived material into the source of the rocks that weathered to form the quartz-biotite schists. Zircon mineral inclusions (quartz, feldspar, apatite, biotite, muscovite and other unrecognized Fe/Al/Si rich phases), along with the major- and trace element contents for the rocks were analyzed to substantiate this interpretation. Together with $\delta^{30}\mathrm{Si}_{\mathrm{NBS28}}$, $\delta^{18}\mathrm{O}_{\mathrm{VSMOW}}$, our results suggest that lithologies like authigenic silica and serpentinized rocks re-melted to form the parent melts that gave rise to zircons found in the USB quartz-biotite schists. Additional Lu-Hf studies reported here on the same zircons also show similarities with NSB zircons. The $\varepsilon_{\mathrm{Hf}}$ values showed a positive correlation with the measured U-Pb age from -22.7 ± 0.8 to +1.9 ± 1.1. The Lu-Hf system also reveals that the USB, extracted at ca. 3.8 Ga, carries isotopic signatures of an older Hadean reservoir, having been formed from an Eoarchean mafic melt that incorporated them. Taken together, this supports a co-genetic origin for the NSB and the USB.

1. Introduction

Although consensus is difficult to come by in any discussion of the Hadean (pre-3.85 Ga) Earth, it is generally agreed that our planet underwent a major silicate differentiation event early in its history (4.4 – 4.5 Ga) (e.g. Boyet et al., 2003, 2005; Caro et al, 2003; Harrison et al., 2008) subsequent to the postulated Moon-forming "Giant Impact" (e.g. Tonks and Melosh, 1993; Nakajima and Stevenson, 2015) and likely after the hypothesized "Late Veneer" at ca. 4.48 Ga (e.g. Mojzsis et al., 2019). It has also been proposed that the magma ocean which cooled from the Giant Impact event created (ultra-)mafic Hadean crust via fractional crystallization (e.g. Caro et al., 2005; Bourdon and Caro, 2007; Rizo et al., 2011). Perhaps at odds with this interpretation, the relatively rapid crustal evolution towards granitoid crust is revealed through study of pre-4.0 Ga (Hadean) zircons (e.g. Maas et al., 1992; Mojzsis et al., 2002; 2014; Harrison et al., 2017; Trail et al., 2018, Turner et al., 2020). A sparse rock and mineral record from the first few hundred million years on Earth, however, means that a better understanding of the nature of early crustal recycling remains elusive. For instance, there is long-standing debate over the operative mechanisms in primordial crustal recycling (Korenaga, 2018); many have advocated what is termed "vertical tectonics" (e.g. Robin and Bailey, 2009) wherein the style of subduction is broadly similar to reverse diapirism. It is noteworthy that this is a mechanism much slower compared to modern subduction zones (Korenaga, 2006; Foley et al., 2014). While a number of workers propose some form of mobile-lid processes in the Hadean (Polat et al., 2002; Furnes et al., 2007; Sleep et al., 2014; Foley and Rizo, 2017), there also exists the view that, the Hadean Earth was under the so-called 'stagnant lid' plate regime (O'Neill and Debaille, 2014; Griffin et al., 2014). The stagnant lid idea shares some dynamical similarities to contemporary Venus wherein lateral lithospheric creep and mantle upwelling contribute to a relatively serene rock cycle punctuated by catastrophic mantle/crust overturn events (e.g. Basilevsky and Head, 2002 and references therein; cf. Rolf et al., 2018). The stagnant lid hypothesis may (or may not) point towards crust foundering as the dominant recycling process on terrestrial-type planets with irregular density contrasts (e.g. Jagoutz and Behn, 2013; Zandt et al., 2004; van Thienen et al., 2004). Argument also prevails over whether plate tectonics as we know it could have initiated in sometime later in the Archean (Shirey and Richardson, 2011; Bédard et al., 2003).

Nearly all that we directly know of the first few hundred million years of Earth history comes from the study of Hadean zircons mostly from the northwestern Narryer Gneiss Complex in Western Australia (Froude et al., 1983; Compston and Pidgeon, 1986). Although these are the oldest earthly materials for which absolute ages are available, it is important to emphasize that the grains are orphaned from their host rocks which either have long since been destroyed, or simply remain undiscovered. Extrapolations made from the mineral geochemistry and inclusion mineralogy of these remarkable zircons has yielded useful insight on the Hadean surface environment (Cavosie et al., 2005; Trail et al., 2016; Bell et al., 2017; Trail et al., 2017; Harrison et al., 2017; Weiss et al., 2018). Considering this sampling handicap, however, any new lading of Hadean/Eoarchean crust has the potential to greatly enhance what we know of this formative time.

Few crustal domains are documented to be older than about 3.7 Ga (King, 2005; Condie, 2019). The oldest generally agreed upon suite of rocks is the Acasta Gneiss in the Slave province, Canada at 3.96 to 4.03 Ga (Bowring and Williams, 1999; Mojzsis et al., 2014; Bauer et al., 2017; Reimink et al., 2018). All known pre-3.65 Ga terranes have experienced protracted and complex metamorphic and deformation histories that make unraveling their history and the chemistry of their parent melts a challenge. A common thread in studies of Hadean/Eoarchean rocks is the challenge of pinning down the absolute timing of their emplacement as well as their parent lithology (protolith). Perhaps the best known such domain is the Isua Supracrustal Belt (Moorbath et al., 1973; Bridgwater and McGregor, 1974) which is a part of the ca. 3000 km^2 Itsaq Gneiss Complex in southern West Greenland (Nutman et al., 1996); only correlative petrographic and geochemical studies at the outcrop scale yield confident results that can be used to assign protoliths (e.g. Cates and Mojzsis, 2006; Manning et al., 2006). More recently, other Eoarchaean (pre-3.7 Ga) supracrustal enclaves were discovered in the North-East Superior Province in Québec, Canada in the Inukjuak domain (Simard, 2003) (**Fig. 1**). Like the Isua locality, the Inukjuak rocks are metamorphosed to upper amphibolite facies that have experienced multiple generations of deformation and have been intruded and surrounded by orthogneisses and mafic/ultramafic sills (Cates & Mojzsis, 2009; Cates et al., 2013; O'Neil et al. 2018). The best studied of these is the Porpoise Cove outcrops of the Nuvvuagittuq Supracrustal Belt (NSB). This locality is an archetype for supracrustal enclaves that are present in the Inukjuak domain (Greer et al., 2020). The NSB is an arcuate sequence of predominantly Ca-poor amphibolitic rocks along with felsic schists, chemical sediments, quartzites, a metaconglomerate and mafic/ultramafic sills that have all been complexly deformed into an open, southwardly plunging synform.

It was previously noted that the NSB is similar in age and in certain geochemical and lithological aspects to parts of the Isua supracrustal belt (Cates & Mojzsis, 2007, 2009; O'Neil et al., 2016). Considering these observations, and a similar evolutionary history laid out by David et al, 2009, it is possible, that these two terranes are the disrupted remnants of what was once a coherent Eoarchean/Hadean block. However, this claim needs further investigation since there are fundamental dissimilarities in the μ^{142}Nd values between the two belts (Saji et al., 2018). Although the NSB has been studied structurally and geochemically, there is no consensus, yet, on its geology, age and origin (O' Neil et al., 2007, 2008, 2013; Dauphas et al., 2007; Darling et al., 2013; Cates & Mojzsis, 2009, 2013; David et al., 2009). Multiple hydrothermal and metamorphic events have masked or erased lithological contacts, altered primary igneous and sedimentary geochemical signatures and disturbed isotopic systems at the local to regional scale (Greer et al., 2020). Some of the prominent debates surrounding the NSB are as follows.

1. The most common rock type in the NSB is a cummingtonite (Ca-poor) amphibolite, with an age of emplacement which remains under debate. Whereas a minimum age limit is established at 3.75 Ga from U-Pb zircon geochronology collected from crosscutting orthogneiss sheets in the supracrustals at the Porpoise Cove locality (Cates and Mojzsis, 2007; Cates et al., 2013; cf. Darling et al. 2013). Significantly, O'Neil et al. (2008, 2012) claim that the emplacement age is Hadean with $^{146/147}$Sm – $^{142/143}$Nd model ages as old as 4.4 Ga and at least 4.115 Ga. This age is based mostly on analyses on the cummingtonite amphibolite, as well as ultramafic/mafic sills arguably structurally discordant to the amphibolite. O'Neil et al. (2012) have also noted a depletion in the μ^{142}Nd and have argued that a partial melting event took place when the ^{146}Sm-^{142}Nd system was still active; i.e., within the first 300 Myr. Other authors have proposed that the model Hadean ages (>4 Ga) instead reflect mixing lines between Archean melt and older Hadean crustal fragments, or an enriched reservoir (Roth et al., 2013; Guitreau et al., 2013; Boehnke et al., 2018). Hints of a Hadean component were shown by Augland and David, (2015) who propose, using Lu-Hf model ages, that the NSB is at least Eoarchean and may be as old as Hadean. Given the large range of reported Nd model ages for the cummingtonite schist from various studies (3.9 – 4.4 Ga) (David et al., 2009; O'Neil et al., 2007; 2008; 2012), it may also be that these reflect a mixture of provenance ages for the sedimentary protoliths (Cates et al., 2013). What is not in dispute is that the Inukjuak rocks experienced thermal events and extensive hydrothermal alteration that affected the Sm-Nd isotopic ratios and thus, possibly, the isochron dates.
2. The NSB comprises a diverse suite of rocks (O'Neil et al., 2007; David et al., 2009; Mloszewska et al., 2012, 2013; Cates et al., 2013; Darling et al. 2013). Although many of these rock units were proposed to have volcano-sedimentary protolith and display extensive hydrothermal alterations including in-place pervasive secondary jaspilite vein development (Greer et al., 2020; cf. Dodd et al. 2017), they remain generally under-explored. Of specific interest are the relatively high whole-rock $\delta^{18}O_{VSMOW}$ values (+6.7 to +11.7‰) for a fuchsite-bearing quartzite reported in Cates et al. (2013) which would support a sedimentary protolith interpretation for these rocks. Yet, this inference was challenged by Darling et al. (2013) with claims that the fuchsite-bearing quartzite is a metasomatized orthogneiss, and that such high δ^{18}O values have been observed in Archean fuchsitic metasomatic systems.

3. Quartz-magnetite rocks identified in the field as banded iron-formations (BIFs) have been analyzed for their δ^{56}Fe (Dauphas et al., 2007) values to establish their chemical sedimentary protolith. Follow-on analyses of mass-independent sulfur isotope fractionations (Δ^{33}S) of the same rocks bolster the claim that these are original marine sedimentary precipitates (Cates et al., 2013; Thomassot et al., 2015).

Given the various studies thus far performed on the Nuvvuagittuq rocks and the ongoing debates over the geology and age of the Inukjuak domain components cited above, it makes sense to compare the NSB to other supracrustal enclaves in the same region. Such work would help to establish (or refute) commonality with the NSB (cf. Caro et al., 2017). These other ubiquitous enclaves (Cates et al., 2009; Greer et al., 2020) are practically unknown to the geological community despite the fact that they could yield important new insights into the global Eoarchean Earth. At the very least, their elucidation would help to put the Inukjuak domain into a clearer context viz. various Eoarchean/Hadean provinces of the North American Craton.

One such enclave that has been noted (Caro et al. 2017) northeast of the NSB (**Fig. 1**) is the informally-named Ukaliq Supracrustal Belt (USB). The USB is enveloped by the same granitoid gneisses of the Boizard suite (2.7 Ga) as those surrounding the NSB (e.g. Saji et al., 2018; Greer et al., 2020) and with a semi-coherent succession of (mafic) amphibolites, ultramafic rocks of probably komatiite origin, quartz-biotite schists, granitoid (principally trondjemitic) gneisses and fuchsite-bearing quartzites (**Fig. 1; Fig. S1**). The USB is an asymmetrical N-S trending elongate metamorphosed volcano-sedimentary succession, and is one of among many of supracrustal fragments and pods of varying size in the region that have been dubbed the Inukjuak Complex (Simard, 2003). Thus far, ^{146,147}Sm-^{142,143}Nd studies show deficits in μ^{142}Nd (Caro et al., 2017; Saji et al., 2018) for some of the Ukaliq amphibolite units much like those of the Nuvvuagittuq area.

Here, we present petrographic thin section studies of select felsic lithological units present in the USB and collected by us in the effort to explore low-T processes that might have affected them. Complementary to this, we present geochemical analyses to constrain the age of the rocks using U-Pb dating of zircons by LA-ICP-MS and secondary ion mass spectrometry (ion microprobe), from targeted samples chosen for their potential to host zircon. Separated zircons from Ukaliq quartz-biotite schists yield the oldest ages recorded, up to 3.79 ± 0.04 Ga. We find that the oldest zircons from the USB are similar in age to detrital zircons documented from the NSB. The ^{207}Pb/^{206}Pb ages of the zircons analyzed cluster at 3.3 Ga, 3.6 Ga, and 3.8 Ga much like the NSB zircons. To reveal additional information about the origin of these grains, *in situ* zircon δ^{18}O and δ^{30}Si measurements were also performed. A new technique that couples measurement of Si and O isotopes (Trail et al.,

2018) was used to help qualify the nature of weathering and alteration experienced by supracrustal material subsequently assimilated into zircon parent melts. The $\delta^{18}O$ and $\delta^{30}Si$ of the zircons suggest that source lithologies that were formed by low to moderate temperature processes (authigenesis, serpentinization, etc.) contributed to the formation of parent melts that crystallized the zircons from the analyzed lithologies. To constrain the emplacement age for these same crystals and the chemical nature and source of their parent melts, Lu-Hf isotope data are also presented. In this way, the emplacement age of the two belts as well as the tectonic setting might be broadly compared. Mineral inclusions in the zircons and the major and trace element composition of the whole rock were studied to explain the nature of the parent melts. Overall, considering the low-T water-rock interactions, our textural and O and Si isotopic observations are consistent with a geologic environment that was suitable for primordial biology to emerge around 3.8 Ga.

2. Sample description

In our work, further rock samples were collected from a variety of lithological units from an area to the north of the study area of Caro et al. (2017) in the region of the Ukaliq belt (**Table 1**) to make comparative textural observations along with geochemical analyses. The rock samples collected from the USB were orthogneisses (I346, I349, I355, I365 and I373), a hornblende schist (I364), a cummingtonite schist (I369) and quartz biotite schists (I370 and I374).

Some samples from the NSB were also collected from which several fuchsite-bearing quartzites (I239 and I240) and are presented herein in order to compare USB and NSB textural observations cited above. It is worth noting that although the USB and the NSB are a few kilometers apart in the Inukjuak domain, they are separated by a shear zone. Superficially, the USB is like the NSB in that it is a sequence of volcano-sedimentary rocks that have been intensely deformed, metamorphosed and intruded as well as surrounded by gneisses; typical for Eoarchean supracrustal enclaves (e.g. Cates and Mojzsis, 2006).

The major lithologies in both supracrustal belts comprise medium to high grade metamorphic rocks. **Table 1** lists the rock types discussed in this study. Particular attention was paid to a fuchsite (Cr-rich mica) bearing quartzite found throughout the NSB. Thin section petrographic analysis was performed on samples of this rock to compare with similar fuchsite-rich quartzites identified in the USB. A previous textural analysis of a fuchsitic quartzite from the Porpoise Cove outcrops by Darling et al. (2013) was used by them to conclude that this rock had an unspecified metasomatic origin from an igneous (granitoid) precursor. All rock types examined herein from both supracrustal localities show both local- (e.g. jaspilite box-veinings; Dodd et al. 2017; cf. Greer et al., 2020) and regional effects of hydrothermal alteration either as alterations of the felsic or the mafic minerals. Different thin sections of the USB rocks display evidence of having been affected differently by fluids even though they represent samples that were collected close to each other or even from the same unit (within several meters). The NSB quartzites share similar characteristics in that the micaceous content of the unit changes from location to location. There are also effects of strain recovery amongst quartz grains of the USB.

3. Methods

3.1 Sample preparation and characterization

Fourteen thin sections were made of four distinct lithological units (Table 1) and investigated by optical and electron microscopy. The latter was conducted with a Zeiss Auriga scanning electron microscope (SEM) at the University of Rochester (USA). The instrument is also fitted with an EDAX X-ray spectrometer with mapping capabilities. The units observed were: orthogneisses, amphibolites and quartz-biotite schists. We also investigated two fuchsite-bearing quartzite samples (I239 and I240) from the NSB equivalent to those reported in Cates et al. (2013) and Darling et al. (2013). The two quartzite samples were collected along strike from the same unit about 10m apart.

Zircons were extracted from five orthogneisses and two quartz-biotite schists following standard heavy liquid techniques. Briefly: hand samples were crushed in pre-contaminated ceramic mortars, reduced to fine sand with pre-cleaned and pre-contaminated ceramic shatter-boxes, sieved, and heavy minerals (including zircon) separated and concentrated with heavy liquids (MEI). The heavy mineral fraction was further conditioned with a hand magnet and passed through a Franz magnetic separator to create a zircon-rich concentrate of low magnetite susceptibility. Individual zircon grains were hand-picked under a binocular microscope and mounted on double-sided tape and cast into 2.55 cm epoxy rounds along with zircon U-Pb geochronology standard AS-3 (Paces and Miller, 1993). In select cases, zircons were also mounted with zircon Si and O isotope standard KIM (Trail et al., 2018). After curing the epoxy, mounts were polished to expose the grain centers using SiC lapping films with a 3 µm grit size, and then finished to a fine polish with a 1 µm film. Zircons were documented by cathodoluminescence and backscattered electron imaging using the University of Colorado JEOL JXA-8230 electron microprobe, at Laboratoire Magmas et Volcans (Clermont-Ferrand, France) with a Scanning Electron Microprobe (SEM), or at UCLA with the UCLA Tescan Vega-3 XMU SEM equipped with a cathodoluminescence detector. Images were collected of these zircons to interpret internal textures (e.g., discern metamorphic growth rims on zircon cores) and, in turn, determine the best location for *in-situ* analysis. Representative BSE and CL zircon images from orthogneisses and quartz-biotite schist samples examined herein are provided in **Fig. 2 & 3**.

3.2 LA-ICP-MS U-Pb geochronology

Zircons from five gneissic and two quartz-biotite schist units from the USB were analyzed on a Photon Machines Analyte G2 193 nm laser ablation (LA) system attached to an Agilent 7900 Inductively Coupled Plasma Mass Spectrometer (ICP-MS) at the University of Rochester. Epoxy mounts were loaded into a HelEx 2 volume chamber that uses He as the carrier gas. The He flow in the HelEx chamber was kept at 0.6L/min and in the HelEx arm at 0.2 L/min. The laser parameters for the analyses are listed in **Table ST1a.** Some of the grains were large enough for multiple analyses; so, where possible, U-Pb measurements were made on a core, intermediate region, and the rim area of the zircon. For zircons that have multiple analyses, the results from the rim and the intermediate region are presented separately from the core analyses. For each analysis, background counts were collected first (~20 sec), following which, the zircons were ablated. Before entering the plasma, the material ablated along with He is mixed with Ar which was introduced at a flow rate of 1.3 L/min. Post ablation, there was a washout period (~20 sec) before moving on to the next analysis. Zircon ages were harmonized against the known AS-3 geochronology standard (Paces and Miller, 1993), and monitored with a secondary in-house standard, Kuehl Lake, believed to be from the same locality as the international zircon standard 91500 (Trail et al., 2018). For the geochronology, the isotopes analyzed were ^{202}Hg, ^{204}Pb, ^{206}Pb, ^{207}Pb, ^{208}Pb, ^{232}Th, ^{238}U, and ^{29}Si. The integration time for ^{206}Pb and ^{207}Pb was 30ms and the for the rest of the isotopes, it was 10ms for each cycle. Silicon-29 was used as an internal standard to determine U and Th concentrations, which were obtained after reduction against NIST612 glass. All data reduction was done with the Iolite 3.32 software package (Paton et al., 2011).

3.3 Ion microprobe Si+O isotopes and U-Pb geochronology.

Subsequent to confirmation by geochronology (Sec. 3.2) that some USB samples host pre-3.7 Ga zircons (I370 and I374), a specific mount was made so that these zircons could be analyzed for their Si- and O-isotopic compositions first. The zircons-of-interest were extracted from two quartz biotite schists samples using the techniques described above (Sec. 3.1) and analyzed using the *ims*1290 ion microprobe at UCLA following the procedures described in Trail et al. (2018). Briefly, a 3-nA Cs+ primary beam, rastering over 20 × 20 μm on the samples, yielded sufficient secondary ion signals (O^{18-} and Si^{30-} $\geqq 6 \times 10^6$ and 3×10^6 counts per second, respectively) to be collected with Faraday cups (FCs) in dynamic multicollection mode. This configuration allows for simultaneous measurement of $^{16}O^{-}$ and $^{18}O^{-}$ on the L′2 and H′2 FCs, respectively, followed by that of $^{28}Si^{-}$ and $^{30}Si^{-}$ on C and H1 (all FCs) after only one mass jump. The mass resolution (M/ΔM) was set at 2,400 (exit slit #1 on the multicollection trolley) to separate molecular interferences from peaks of interest. One spot analysis is composed of 14 cycles, each of which includes a counting time of 10s for oxygen isotopes, and of 15s for Si isotopes. The backgrounds of FCs were determined during the 90s pre-sputtering before each analysis, and then were corrected for in the data reduction.

After the completion of stable isotope measurements, the surfaces of the samples were gently re-polished with special care taken to preserve the location of the Si + O isotope measurement as visible analysis pits, and then re-coated with Au in preparation for ion microprobe geochronology. The U-Pb ages for this subset of zircons were determined on the CAMECA ims1270 ion microprobe at UCLA using a ca. 15 nA primary O^- beam generated from the duoplasmatron focused to a ca. 20 µm spot at a mass resolving power of 5000 (e.g. Bell et al., 2017; Quidelleur et al., 1997). To increase Pb sensitivity the analysis chamber was flooded with oxygen. Zircon U-Pb ages were standardized against AS-3, and most likely source of common Pb contamination was from sample preparation. Thus, all data were corrected for common Pb contamination using Pb isotope data reported for California surface waters (Sañudo-Wilhelmy and Flegal 1994). Note that the ion microprobe geochronology was conducted *after* Si and O isotope investigations to prevent contamination of exogenous O in zircon from the primary ion source. For these samples, the ion microprobe was used in preference to the LA-ICP-MS to preserve enough of the grain for Lu-Hf analyses.

3.4 Lu-Hf

The Lu-Hf isotope analyses were performed at LMV (Laboratoire Magmas et Volcans, Clermont-Ferrand, France). Details regarding operating conditions are available in **Table ST3**. Zircons were analyzed in batches of 10 unknowns (4 standards and 6 samples) bracketed by the synthetic MUN zircon standard, which is doped in heavy REEs (MUN-0; Fisher et al., 2011). Standards analyzed as unknowns (91500, MudTank, and two MUN zircons with low and high Yb/Hf ratios) served as quality control. For zircons from Ukaliq samples reported herein, Lu-Hf spots were located on the trace pits of previous U-Pb measurements. Both Yb and Hf instrumental mass biases were determined using $^{173}Yb/^{171}Yb$ normalized to the value of 1.129197 (Vervoort et al., 2004) and $^{179}Hf/^{177}Hf$ normalized to 0.7325 (Stevenson and Patchett 1990). The Lu fractionation was assumed to follow that of Yb (Fisher et al., 2014), and values of 0.793045 for $^{176}Yb/^{173}Yb$ (Vervoort et al., 2004) and 0.02655 for $^{176}Lu/^{175}Lu$ (Fisher et al., 2014) were used to remove isobaric interferences of ^{176}Yb and ^{176}Lu at mass 176. We carefully monitored each time-resolved signal to minimize issues of domain mixing and grain heterogeneities. Owing to the fact that Hf isotope standards tend to show a slight shift in $^{176}Hf/^{177}Hf$ after mass bias correction, we have used MUN-0 to determine an offset factor and correct all LA-MC-ICP-MS analyses for this mismatch. Results obtained on standards comport well with consensus values. The average $^{176}Hf/^{177}Hf$ measured in 91500 and MudTank were, respectively, 0.282307 ± 0.000041 (2 std; n = 7) and 0.282495 ± 0.000035 (2 std; n = 6), which agree well with consensus values of 0.282308 ± 0.000008 (Blichert-Toft, 2008) and 0.282507 ± 0.000006 (Woodhead and Hergt, 2005). The average ^{176}Hf/^{177}Hf measured in MUN_1-2b and MUN_4-2b were 0.282133 ± 0.000037 (2 std; n = 7), and 0.282126 ± 0.000018 (2 std; n = 6) respectively, therefore fully consistent with the value of 0.282135 ± 0.000007 reported in Fisher et al (2011). We have used the ^{176}Lu decay constant value of Scherer et al. (2001) and Söderlund et al. (2004), which is 1.867 x 10^{-11} yr^{-1}, to calculate initial Hf isotopic compositions. Uncertainties associated with the radiogenic-ingrowth correction were propagated using the algorithms of Ickert (2013). Finally, ε_{Hf} values were calculated using CHUR values provided in Iizuka et al. (2015).

3.5 Major and Trace elements

Chips of two quartz-biotite schists (I370 and I374) were sent out to Hamilton Analytical Laboratory, Clinton, NY (USA) to characterize major and trace element contents by X-Ray Fluorescence (XRF) spectrometry. The chips were chosen for minimal alterations and were visibly as devoid of saw marks as possible. Before processing the samples, saw marks were removed so that residual metal saw particles would not interfere with the measurements. Chips were then milled to a fine powder using a Rocklabs tungsten carbide (WC) or alumina ring mill and fused with a Li-tetraborate flux in a graphite crucible at 1000 °C to form a pellet. These pellets are cleansed of residual carbon, reground and fused again at 1000 °C. The resulting pellets were polished using diamond laps to create polished pellets 29mm in diameter which were then analyzed using the Thermo ARL Perform'X XRF spectrometer.

3.6 Mineral Inclusions

Several zircons from two quartz-biotite schists (I370 and I374) were imaged using a Vega 3XMU scanning electron microscope (SEM) at UCLA. Both EDS and WDS X-ray spectroscopy were performed on the SEM and a JEOL 8600 Electron Microprobe respectively to identify mineral inclusions in the zircons. The inclusions were classified in three separate groups. First, some inclusions were classified as “isolated”; i.e., they were not in contact with any cracks and are thus considered primary. The second group of inclusions is classified as is “possibly secondary minerals” as they were associated with cracks, which are avenues of fluid intrusion. Third, those assigned as “crack-filling inclusions” are most certainly secondary. The counting protocol employed, which characterizes the diversity of inclusions found, is that established by Bell et al., (2015) and Bell, (2016) where the mere occurrence of a phase in a zircon is regarded as a single occurrence regardless of the number of inclusions. For example, three crack-isolated apatite inclusions in a single zircon contributes to a single count of crack-isolated apatite inclusions (Bell et al., 2018). The comprehensive list of inclusions detected is summarized in **ST4**.

4. Results

4.1 Thin section observations

To summarize, the major lithologies are medium- to high-grade metamorphic rocks that range from biotite schists to amphibolites all the way up to hydrous mineral bearing high-grade gneisses (**Fig. 4 a-c**). A biotite-fuchsite bearing quartzite unit was also sampled from the NSB as a point of comparison with regards to hydrothermal alteration in the Inuakjuak domain (**Fig. 4d**). All these rock types show effects of hydrothermal alteration either as alteration of the felsic or the mafic minerals or deposition of secondary minerals or both.

4.1.1 NSB Biotite-fuchsite bearing quartzite from the NSB (I239 and I240)

This study samples two sections of a coarse-grained metamorphic rock from the NSB that is predominantly quartz with minor plagioclase occurrences (I239 and I240) (**Fig. S2 d**). Quartz grains show grain boundary migration and sub-grain formation. The plagioclase has been altered to sericite. Fuchsite is present along the margins of the felsic grains but do not show distinct parallel foliation. One of the sections (I239) contains a greater proportion of fuchsite and biotite even though they are from the same rock unit. This terrane is non-uniform in terms of its pattern of hydrothermal alteration. Both these sections contain as accessory phases, chromites, monazites and zircons. Consequently, we view the likely protolith of this rock as a detrital sand rich in heavy minerals.

4.1.2 USB Quartz-biotite schists (I370 and I374)

These rocks are medium- to coarse-grained metamorphic rocks with continuous schistosity defined by mafic and felsic layers (**Fig. S1a**). The mafic layers are defined by biotite that has been altered by varying degrees to chlorite, Fe/Ti-oxides/sulfides and/or rutile (**Fig. S1b & c**). The layers show rough foliation where the biotite crystals are disjoint grains. These micaceous minerals have inclusions of apatite, zircon and monazite identified by radiation halos. The felsic domains comprise anhedral to subhedral grains of plagioclase and quartz. In some sections, the plagioclase shows deformation twinning, and the grain boundaries of both quartz and plagioclase are defined by a fine-grained matrix of mica and similar phases as the felsic domains. This is probably the result of a combination of hydrothermal alteration and recrystallization through pressure solution where grains having sharp edges with low surface area are in contact thereby leading to high pressure regions. This causes material to be displaced from these regions to surrounding low pressure regions. The quartz in all sections shows grain boundary migration and sub-grain formation with abundant triple-junctions with pinning by accessory minerals (**Fig. S1d & e**). Some of the felsic grains contain inclusions of mica which could be foliation from a previous generation of deformation or relict grain boundaries that have been consumed by mineral growth (**Fig. S1e**). There are also inclusions of quartz in many plagioclase crystals which may be myrmekitic or an effect of re-melting and recrystallisation of feldspar. More detailed SEM investigations have revealed the presence of monazite, native Pb, allanite, and titanite.

4.1.3 USB Amphibolites (I364 and I369)

Two kinds of amphibolites were identified: a hornblende-bearing (Hb-amphibolite; **Fig. 4e**) (I364) and a cummingtonite-bearing (low Ca) type (Cum-amphibolite; **Fig. 4f**) (I369). Both show signs of alteration with the hornblende being extensively altered to chlorite, biotite and Fe/Ti-phases and the cummingtonite is sparingly altered to not altered at all. The amphiboles mentioned define the mafic layers of all the schists. In the Hbl-amphibolite, biotite crystals flow around porphyroblasts (**Fig. S1f**) (no fine-grained matrix surrounding the porphyroblasts) suggesting that they developed after the plagioclase formed. The texture of the cummingtonite-amphibolites changes from one thin-section to another. The grain size reduces, and the grains are more disjoint from one to another. The felsic domains comprise plagioclase and quartz where the plagioclase crystals have been partially sericitized. Observations made under an SEM show titanite, ilmenite, rutile, and zircon.

4.1.4 USB Granitoid (ortho-)gneisses and granitic gneisses (I346, I349, I355, I365, and I373)

The sampled granitoid gneisses are all mica-bearing tonalitic (I346 and I355) or granitic gneisses (I349 and I365) (**Fig. 4a**). They are medium to coarse grained and the minerals are subhedral to anhedral. There are both felsic and mafic minerals in all rocks sampled. The minerals are dominantly plagioclase, quartz, alkali feldspar in some rocks and biotite. There are accessory phases such as apatite and zircon present as inclusions in the biotite. The biotite has also been hydrothermally altered in multiple locations to chlorite and Fe/Ti ore phases. In certain sections, the plagioclase has not been altered while the biotite has (**Fig. S2a**). In some other sections the opposite has been observed (**Fig. S2b**). In the granitic gneisses there are both alkali feldspar and plagioclase. In certain locations, myrmekite textures are visible on the border of two feldspars. The tubular quartz might be considered evidence for metasomatism (**Fig. 4i**). In all the gneisses, the quartz grains show recovery and recrystallisation by bulging, grain boundary migration and sub-grain formation. In some locations, the quartz shows ribboning.

In one of the sections (I373), anhedral alkali feldspar grains in some locations are surrounded by plagioclase (**Fig. S2c)**. This may either be because alkali feldspar transformed to plagioclase or because the alkali feldspar is secondary and crystallized from infiltrating fluids. SEM investigations reveal zircon, ilmenite, monazite, and xenotime.

4.2 USB U-Th-Pb Geochronology (LA-ICP-MS and SIMS)

The ^{207}Pb/^{206}Pb ages of zircons and their Th/U ratios are summarized in **Table 2** (Complete dataset in **Table S1b**). The latter can be used cautiously as an indication whether the analysis sampled a metamorphic zone in the zircon (e.g., Mojzsis and Harrison, 2002; Rubatto, 2002). Metamorphic zircons generally have widely variable Th/U; i.e., <0.001 or >10 (e.g., Yakymchuk et al., 2018), whereas igneous zircons tend to have values around 0.8 (e.g., Kirkland et al., 2015). Thus, Th/U as a differentiating parameter is better used in conjunction with CL and BSE images to consider whether zircon domains are more consistent with igneous or metamorphic processes. Upon observing the zircons from the gneisses and the schists, noticeable differences appear. Zircons from both rock types show oscillatory zoning in the core but the zircons from the quartz-biotite schists have a more regularly occurring and prominent growth rims (**Fig. 3**). The gneiss zircons either have very thin or non-existent rims. The Th/U ratio of the core of the gneiss zircons have a greater spread (0.02 – 1.48) compared to the schist zircons (0.02 – 0.74) (**Fig. 5**) but they have a similar Th/U ratio at an average of 0.4 compared to the schist zircons at 0.45. This is dissimilar and opposite to the observations made on the NSB units (Cates and Mojzsis, 2007) both in terms of spread and absolute values (**Fig. 6)**. The zircons from the NSB gneisses, analyzed by Cates and Mojzsis, 2007, have a smaller spread (0.01 – 0.85; average = 0.54) compared to the quartz-biotite schists (0.03 – 2.19; average = 0.65). Thus, on average, based on the CL images and the Th/U ratios, zircon cores in the USB orthogneisses or schists are consistent with a magmatic origin. The analyses considered when assigning ages for each of the rock units, based on zircon U-Pb geochronology, (**Table 2**) were analyses with U-Pb concordance between 90 and 100% and closest to the core of the grains. These grains have been presented on a concordia diagram (**Fig. S3)**. The age histograms, on the other hand, (**Fig. 5 & 6**) present grains with % discordance

$(1 - \frac{Pb^{206}}{U^{238}} / \frac{Pb^{207}}{U^{206}}) * 100$ between -10 and 10.

4.2.1 USB orthogneissic units (I346, I349, I355, I365 and I373)

The ^{207}Pb/^{206}Pb ages for the gneissic zircons, when categorized based on their host rock and averaged – except for I373 – range from 3.26 to 3.34 Ga. When the ≤10% discordant zircons are plotted on a concordia diagram (**Fig. S3a**), most of them cluster between 3.5 and 3.0 Ga implying that this time period accounts for most of the sampled igneous non-disturbed zircons. The youngest age for a zircon is from I355 at ca. 2.4 Ga. This analysis also has a very high Th/U ratio at 1.49 which might point to Pb loss. The I373 zircons need to be mentioned separately because of all the analyses on zircons from this unit, only two analyses of the intermediate region between the core and the rim is between 90 and 100% concordant. The maximum I373 zircon age is 3.68 ± 0.07 Ga which may be considered as the emplacement age of the orthogneisses.

4.2.2 USB quartz-biotite schists (I370 and I374)

The ages obtained from the zircons of the USB schists are between 2.73 – 3.77 Ga which is like the quartz-biotite schists of the NSB (3.5 – 3.8 Ga) (David et al., 2009; Cates et al., 2007, 2009 and 2013). The maximum ages of zircons from the two quartz-biotite schists are 3.78 ± 0.08 and 3.79 ± 0.04. This implies that the protoliths of these schists incorporated material that is at least about 3.8 Ga. Zircons from these schists were also measured using SIMS which gave much more precise maximum ages at 3.76 ± 0.01 and 3.74 ± 0.01 (2 s.e.) Ga. The quartz-biotite schist analyses show a distribution with a mode at around 3.7 Ga with a few outliers around 2.7 Ga. Some of the outliers have a degree of concordance below 90% implying Pb loss. Younger ages, defined here at 2.7 Ga, have corresponding low Th/U ratio (~0.1 – 0.01) when compared to older (<3.0 Ga) ones. The concordant zircons that have been analyzed with an LA-ICP-MS show a tight cluster at ~3.6-3.8 Ga (**Fig. S3b).**

4.2.3 Zircon zonal analyses

Zircons from some of the gneisses were analyzed zonally; i.e. the core, intermediate, and rim sections of zircons from individual gneissic units. All the values from each of the zones were averaged to investigate at the variation in the age and Th/U ratio within a single average zircon grain (**Fig. 7**). For most of the units, the ages of the zones are similar (~3.3 Ga) except for I365 (Gneiss) which has rim and intermediate ages (~3.45 Ga) greater than core ages (~3.1 Ga), but this may be because the I365 grains have more cracks than grains from other units. The Th/U ratio of the rim measurements for some of the rocks (I349 and I355) is also lower than the core values.

4.3 In-situ Si and O isotopes in USB zircon.

The zircons from the two quartz biotite schists (I370 and I374) are well scattered both in terms of δ^{18}O and δ^{30}Si, with latter values of both units having a larger range from -0.07 to -0.75 ‰. Most of the zircons are indistinguishable from the δ^{30}Si mantle values of -0.38 ± 0.02 ‰ (**Fig. 8**). Zircons from both samples show δ^{18}O (relative to VSMOW) to be distinct from the mantle value of 5.3 ± 0.3 ‰, with values that range from 5.6 to 6.6 ‰ (**Table ST4**). All data collected are reported but of all the zircons measured for their isotopic values (**Table ST4**), only the ones for which the analytical location of the ion microprobe spot did not hit a crack, or an inclusion (determined using SEM images) are discussed in detail. The rejected values are not anomalous from the rest of the dataset except for a couple of analyses that show sub-mantle values for both isotopic systems. The samples that were rejected was done so because we found cracks in the analysis location post-sputtering.

4.4 Lu-Hf in USB zircon

Zircons separated from quartz-biotite schists (I370 and I374) were analyzed for their Lu-Hf isotope systematics and corresponding data are reported in **Table ST7**. These data have been acquired as a means of comparison between the NSB and the USB, and to discuss the sources of zircon parental melts. The Lu-Hf isotopic system in zircon is particularly effective in obtaining the Hf isotope composition of the source to zircon parent melt since this mineral incorporates substantial amounts of Hf (up to 1 wt%) whereas it only accommodates a minimal amount of Lu. This leads to minimal growth of radiogenic ^{176}Hf over time; thus, the present-day ^{176}Hf/^{177}Hf ratio of the zircon very closely resembles the ^{176}Hf/^{177}Hf ratio of the parent melt from which it crystallized. The ^{176}Lu/^{177}Hf ranges between 0.000428 ± 0.000018 and 0.001126 ± 0.000018. The ^{176}Hf/^{177}Hf ratio varies between 0.280304 ± 0.000021 and 0.280413 ± 0.000031. For both these ratios, the scatter is similar to that of previous studies performed on the zircons from the NSB (**Fig. 10a & b**). Finally, the initial ε_{Hf} ($\varepsilon_{Hf(t)}$) range from -22.7 ± 0.8 to +1.9 ± 1.1 and data altogether define a positive correlation between $\varepsilon_{Hf(t)}$ and ^{207}Pb/^{206}Pb ages.

4.5 Major and trace elements of I370 and I374 (USB).

The major element data is plotted along with the NSB quartz-biotite schists (IN05004, IN05005, IN05020, IN05037, IN08036) of Cates et al. (2013) (**Fig. 11**). This was done to look for any trends and similarities when plotted as Harker diagrams. Any subsequent and inferred trends provide supporting evidence that NSB and USB schists might be consanguineous. Also, major element compositions for averaged Witswatersrand shales (WS) (Wronkiewicz and Condie, 1987), metasediments from the Isua supracrustal belt (MISB) (Bolhar et al., 2005) and Archean platforms/shields (APS) (Rudnick and Fountain, 1995) are presented alongside the schists from the USB. The WS is an Archean mafic shale, thus comparisons were made to qualify the felsic nature of the USB schists while the Isua and the Archean platforms data is presented to act as a point of comparison between Archean terranes. Trace element spider diagrams, normalized to the NASC (North American Shale Composite) (Gromet et al., 1984), are presented for schists from the USB along with the mafic averaged Witswatersrand Shales, Isua metasediments and Archean platforms for reference (**Fig. 10**). The NASC is supposed to represent the average upper continental crust trace element composition. The measurements show that the rocks are high in SiO_2 (~70%) and low in mafic oxides MgO, Fe_2O_3, MnO and TiO_2 (~2%, ~3.5%, ~0.035% and ~0.35% respectively) compared to the apparently more mafic NSB rocks, the WS, MISB and the APS.

The CaO and K_2O contents of the NSB and USB schists are comparable while the USB Na_2O content is higher. When the NSB and USB rocks are plotted together in Harker diagrams, MgO, Fe_2O_3, TiO_2, Al_2O_3 and K_2O show inverse correlations while only Na_2O arguably shows a positive correlation. The mafic oxides (MgO, Fe_2O_3, MnO and TiO_2) are also plot against Al_2O_3 and except for TiO_2, which shows a strong correlation, they show a weak to moderate positive correlation. The trace element measurements have been presented as a comparison between the USB and the NSB while the other Archean lithologies act as points of reference~~.~~ The entire major and trace element data set is presented in **Table ST8.**

5. Discussion

Eoarchean supracrustal rocks are a rare commodity, possibly because during their long (>3.6 Ga) crustal residence times they have been lost due to erosion combined with some form of crustal recycling. Those that remain have – without known exception – undergone extensive metamorphism and deformation. Such a history has all but erased primary textures and thus has made understanding the surface processes active on Earth prior to 3.6 Ga, vague. Given the present-day close association of the NSB and the USB, a reasonable question is whether and to what extent these Eoarchean supracrustal sequences share any similarities, or on the other hand, if they have differences, what new information is revealed about the Eoarchean Earth? Common themes among the two belts include hydrothermal alteration, secondary mineral deposition, similar metamorphic grades and lithologies, similarities in U-Pb ages and Lu-Hf isotopic ratios.

5.1 General texture of the Inukjuak rocks

The NSB fuchsite-bearing quartzite (I239 and I240) has a chaotic fuchsite pattern that is not restricted to uniform and regular layers but rim the felsic grains which implies that the fuchsite might have been a later hydrothermal deposit. Since this rock is a quartzite, its protolith is most probably a sedimentary rock, yet the outcome of the work of Darling et al. (2013) claims an igneous protolith. Most authors prefer Archean fuchsite-bearing quartzites to have an uncomplicated origin from sedimentary protoliths (Raza et al., 2010; Maier et al., 2012; Nutman et al., 2014). Similar debates might arise when the USB is studied in detail; such debates might likewise require comparative studies. Our observations are consistent with the scenario that the Cr in the micas is likely derived from the partial dissolution of chromites documented to present in the quartzite. Electron imaging has revealed chromites showing a thatched texture surrounded by fuchsite (**Fig. S6**) which lends supports this interpretation (Cates et al., 2013). Since chromite is generally not a primary phase in a granitoid, the protolith of these rocks are more likely to be sedimentary and not a metasomatized orthogneiss as postulated by Darling et al. (2013).

Different thin sections like the orthogneisses (I346, I349, I355, I365 and I373) have evidence of different degrees of hydrothermal alteration even though they represent samples that were collected close to each other, or even from the same unit. In some sections, we observe in thin section that the plagioclase is altered while the biotite is relatively pristine while in other samples, the opposite is observed. The NSB quartzite shares similar characteristics with the USB quartz-biotite schists in that the micaceous nature of the unit changes from location to location. There are also effects of strain recovery amongst quartz grains. The quartz-biotite schists are unlike those of the NSB in that they do not contain any porphyroclasts of quartz that have led authors to suggest that the NSB schists might be metaconglomerates (Cates and Mojzsis, 2007). Apart from this dissimilarity they are similar in metamorphic grade and mineralogy. The amphibolites and gneisses show moderate to extensive hydrothermal alteration of the mafic minerals implying metasomatism, while the quartz grains show grain boundary migration, subgrain formation and even ribboning in certain locations (**Fig. 6**), like the NSB. The ribboning suggests that the gneisses experienced crystal-plastic deformation. The presence of cummingtonite amphibolites is also a different observation from that made by Caro et al. (2017) on a part of the belt further south with difference exposure, who observed that such rocks are rare in the USB. Some of the gneisses (I346; oldest zircon age: 3.50 ± 0.05 Ga and I349; 3.49 ± 0.04 Ga) show myrmekite textures which indicate hydrothermal alteration. Coupled observations made on mafic and felsic minerals in various gneissic sections imply both a K-deficient fluid (chloritized biotite and relatively unaltered plagioclase) and a K-saturated fluid on a different thin section (sericitization of plagioclase but unaltered biotite) (**Fig. S2c**). Based on these observations and similarities with the NSB the protolith for the USB quartz-biotite schists are consistent with a sedimentary origin (Greer et al., 2020). These observations pointing toward extensive and varied metasomatism is corroborated by Caro et al. (2017) who documented a high degree of serpentinization in southern section of the USB. The alterations are evidence that both supracrustal belts experienced hydrothermal alteration.

5.2 Evolution of the Inukjuak Domain: U-Pb geochronology, CL and BSE images and internal zoning of USB zircons

Several timelines for the evolution of the Inukjuak Domain have been proposed that use different geochronological techniques applied to the NSB (Cates and Mojzsis, 2007, 2009; David et al., 2009; O'Neil et al., 2008, 2012, 2016). While ^{142}Nd/^{144}Nd isochron ages of multiple units as well as negative μ^{142}Nd values (up to -18 ppm for cummingtonite amphibolites; O'Neil et al.,2012) have been used to argue that the NSB has a Hadean formation age (O'Neil et al., 2008, 2012 and 2016). This conclusion has not been corroborated by other systems like the ^{147}Sm-^{143}Nd and the ^{176}Lu-^{177}Hf which report the formation ages to be Eoarchean (Roth et al., 2013; Cates et al., 2013; Guitreau et al., 2013), which is in turn supported by the in-situ U-Pb ages from Cates and Mojzsis, (2007) and David et al. (2009). However, O'Neil et al. (2012) measured some mafic sills intruding into the cummingtonite amphibolites to find their $^{143}Nd/^{144}Nd$ isochron ages are Hadean which according to them sets the minimum age of the NSB at 4.1 ± 0.1 Ga. We emphasize, however, that the general de-coupling between these chronometers was previously explained by Roth et al. (2013) to be a result of an Eoarchean thermal event that caused the resetting of Nd isotopic ratios. As such, an accurate extraction age *cannot* be obtained using the Sm-Nd chronometers. The "Hadean" model age and the negative $\mu^{142}Nd$ have been explained by authors to be signatures from remnant Hadean crustal fragments or an enriched mantle source (Roth et al., 2013; Cates et al., 2013; Boehnke et al., 2018). Guitreau et al. (2013) has also suggested the re-fertilization of the mantle source that created the NSB.

Before making inferences about the ages measured on our zircons, they need to be identified and confirmed as igneous (emplaced) rather than hydrothermal/metamorphic (neoform). The zircons discussed in this study all show oscillatory zoning in the grain core, consistent with an igneous origin. Our age range from five different gneissic units is between 3.26 and 3.68 Ga. This implies that the USB records multiple generations of magma formation or that the younger ages might possibly be recording a later metamorphic event or be artifacts of metamorphism. The latter may not be the case because in reporting the average or emplacement ages, highly concordant zircons were selected (<10% discordant). The oldest ages from the gneisses range from 3.47 – 3.68 Ga which, if considered as an emplacement age for the protolith, are younger than the oldest ages reported for the NSB. This could mean that the NSB gneisses record an earlier generation of zircon crystallization. However, this would not be the case if the USB zircon ages mentioned above are not igneous. The average Th/U of the gneissic zircons range between 0.26 and 0.6 which is consistent with a zircon having an igneous origin. The Th/U values however do not have a tight cluster (**Fig. 5**) which could be because the zircons retain a record of metamorphism. The orthogneiss zircons analyzed by Cates and Mojzsis, (2007) also have similar Th/U ratios between 0.51 and 0.74. In their depth profiling study, Cates and Mojzsis, 2009 obtained Th/U ratios of 0.41 and 0.31 from the core of the two zircons that they analyzed from a TTG unit. This is close to the values for our grains.

Two quartz-biotite schists were analyzed in this study (I370 and I374). The oldest grains have ages of 3.78 ± 0.08 and 3.79 ± 0.04 Ga from the corresponding units. When compared to the zircons analyzed by Cates and Mojzsis, 2007, our zircons seem to be slightly older than those from the NSB quartz-biotite schists. Since these older rocks do not possess porphyroclasts as the quartz-biotite schists of the NSB, these units might be a completely new unit discovered in the region and might have experienced different environments from the lithologically similar rocks in the NSB. The difference is observed in the

Th/U values as well. The zircons analyzed by Cates and Mojzsis, 2007 from quartz-biotite schists (IN05020 and IN05037) in the NSB show a greater range in Th/U which might mean a more inhomogeneous parent melt or sampling of multiple parent melts. The average Th/U ratio of both the USB units is 0.44 ± 0.06 and 0.52 ± 0.07 which seems to be in line with a magmatic origin. The Th/U ratios of the USB zircons do not have a large spread (**Fig. 6**) which is consistent with a more homogenous parent melt. The oldest U-Pb age thus far reported is 3.82 ± 0.02 Ga which is an upper intercept age on a Wetherill Concordia diagram. This was determined by David et al. (2009) from a group of six zircons from a quartz-biotite schist using the ID-TIMS method. This age is comparable to the minimum emplacement ages presented for the gneisses from the NSB at 3.75 ± 0.01 Ga (Cates and Mojzsis, 2007) which suggests that these two rock types might be coeval. This observation has also been made for rocks from southern West Greenland (Nutman et al., 2004) where Archean orthogneisses and metasediments contain zircons that range in age from 3.65 to 3.9 Ga. The ages reported here also overlap the ages for a clast-free pelitic schist from the Isua Supracrustal Belt; which is 3.78 ± 0.01 Ga (Nutman et al., 1996).

Finally, we would like to mention that we consider the maximum depositional ages for both schist samples to be around 3.65 Ga, and not that of the oldest zircon grains. This is because the Th/U and the % concordance are 0.43 and 100. Also, the CL and BSE images of I370_3_7 reveal distinct oscillatory zoning consistent with (but not proof of) an igneous origin (**Fig. S7**). The laser-ablation age for this grain is 3.65 ± 0.06 Ga. Any zircons that are younger than this age, have been affected by Pb-loss and show a 100% concordance. There are older zircons showing magmatic features and greater concordance but if they were to designate depositional ages, then I370_3_7 should be classified as metamorphic which is hard to argue given the oscillatory zoning that it possesses.

5.3 Lu-Hf isotopes

Similar to the overall objective of the study, Lu-Hf systematics was used to establish similarities or differences between the rocks of the NSB and the USB, as well as to deduce information about their formation and evolution. Zircons in this study have been compared to NSB in terms of the chemical nature of the host rock sources and the location of the source. Zircons and whole rocks from the NSB have been analyzed for their isotopic ratios so there exists a substantial database against which comparisons may be made. **Fig. 10** shows that data from this study have similar Hf isotope signatures, U-Pb ages, and, hence, evolutionary pattern to NSB data from previous studies (Guitreau et al., 2012, 2013; O'Neil et al., 2013; Augland and David, 2015). This observation strongly suggests a shared history between USB and NSB.

The evolutionary pattern is similar to what would be observed if U-Pb ages were affected by ancient disturbances as argued by the good match between the general correlation and the evolution lines corresponding to measured $^{176}Lu/^{177}Hf$ in zircons (0.0004-0.002; **Fig. 10a and 10b**). Moreover, precise ID-TIMS ages reported in Augland and David (2015) clearly indicate that non-zero-age disturbance occurred in the NSB much like what is often seen in Archean zircons (e.g., Patchett, 1983; Gerdes and Zeh, 2009; Guitreau et al., 2012, 2019). This results in U-Pb ages being younger than that of their actual crystallization and associated ε_{Hf} values being artificially too low (e.g., Guitreau and Blichert-Toft, 2014). Therefore, this consideration together with the fact that CL images display metamorphic recrystallization textures would argue in favor of some of the datapoints representing this artifact. We estimate the maximum depositional age of I370 and I374 being around 3.65 Ga and, hence, consider that zircons older than this are magmatic and all those younger are artifacts of ancient U-Pb disturbance.

The zircon data presented by other authors, especially O'Neil et al. (2013), nevertheless, illustrate that this seemingly artificial correlation (**Fig. 10b**) is similar to that exhibited by data for magmatic zircons, and hence, represents the true evolutionary pattern of NSB and USB zircon-bearing rocks (**Fig. 10d**). This slope is equivalent to a $^{176}Lu/^{177}Hf$ typical of TTGs such as those present in the NSB. O'Neil et al. (2013) argued that the slope is too steep to be accounted for by the NSB only being made of Archean rocks, and used it as an evidence for the presence of Hadean rocks in the NSB. In fact, these authors assumed that the slope should be equivalent to a $^{176}Lu/^{177}Hf$ typical of a basaltic rock because TTGs are reworking products of metabasalts (e.g. Moyen and Martin, 2012). Although, this reasoning has some petrological logic on a first order, the slope of such pattern cannot be interpreted at face value because, in practice, seemingly simple evolutionary patterns can hide complex petrological processes that are geochemically buffered by dominant enriched crustal lithologies. This was well illustrated recently by the work of Laurent and Zeh (2015) who showed that felsic rocks of the Pietersburg block (South Africa) define a simple evolutionary pattern in a ε_{Hf} versus age diagram despite these rocks being formed in various geodynamic contexts and from several distinct sources. As a consequence, the combined NSB-USB evolutionary pattern can merely be interpreted as being buffered by dominant ~3.7-3.8 Ga granitoids of TTG affinity because the slope defined by data in **Fig. 10d** is equivalent to that of the felsic lithologies in the NSB ($^{176}Lu/^{177}Hf = 0.002$; Guitreau et al., 2012, 2013) and fully consistent with TTGs worldwide (Guitreau et al., 2012). Furthermore, the near-chondritic initial Hf isotope signature of the 3.7-3.8 Ga zircons comply very well with that of global TTGs (e.g., Guitreau et al., 2012 and references therein). Finally, the Hf isotope signatures of NSB amphibolites (**Fig. 10d**) are consistent with the 3.7-3.8 Ga TTGs being generated by the reworking of these amphibolites, which was demonstrated experimentally by Adam et al. (2012) who essentially reproduced earlier experiments on TTG petrogenesis (e.g., Rapp and Watson, 1995). In a nutshell, available Hf isotope data do not require the involvement of a Hadean reservoir to account for the evolutionary pattern of NSB and USB, and the following magmatic history can be outlined:

1- Extraction of mafic rocks equivalent to amphibolites in the NSB and USB around 3.8 Ga;
2- Reworking of some of these mafic rocks to form the protolith of felsic gneisses (1st felsic generation) between 3.7 and 3.8 Ga;
3- Deposition of the protolith of the quartz-biotite schists at 3.65 Ga and reworking of existing lithologies (mafic and felsic) to generate the Voizel tonalites (2nd felsic generation; Greer et al., 2020) between 3.45 and 3.65 Ga that have Hf isotope signatures buffered by gneisses of the 1st felsic generation.
4- Further reworking and/or buffering during the Boizard granite formation 2.7-3.0 Ga (3rd felsic generation) (Greer et al., 2020).

However, ^{142}Nd anomalies require the presence of a Hadean enriched reservoir, possibly crustal, somewhere in NSB and USB history (O'Neil et al., 2008). Much like what is proposed in Guitreau et al. 2013, Boehnke et al., 2018 and Caro et al., 2017, we suggest that the involvement of the Hadean crust dominantly, if not exclusively, took place during the mafic crust formation around 3.8 Ga. The signature of this Hadean crust was transferred to granitoids during a second-stage process corresponding to mafic crust reworking. The range of chemical and isotopic values exhibited by NSB/USB amphibolites can account well for the evolutionary pattern and incorporated Hadean crustal signatures in multiple isotopic systems (Sm-Nd, Lu-Hf; O'Neil et al., 2008, 2017; Guitreau et al., 2013; Caro et al., 2017), as well as in its chemistry (Adam et al., 2012; Boehnke et al., 2018, Caro et al., 2017).

5.4 Si+O isotopes in zircon: preservation of primary signatures and implications for source.

The coupled measurement of Si and O isotopes of zircons is a new technique being applied to the rocks of the Inukjuak domain, and we apply these measurements to zircons found in quartz-biotite schist samples, which have the oldest reported ages. To our knowledge, only whole rock O isotope measurements of fuchsitic quartzites from the NSB have been made (Cates et al., 2013). While rocks from the USB preserve direct evidence of hydrothermal activity at 3.8 Ga or later, information can be obtained from zircons about parent melts though stable isotope investigations. Coupled δ^{30}Si and δ^{18}O measurements can reveal the clues about protolith that hosted these zircons; specifically, the lithologies that melted to produce the melt that formed the protolith. This is because both Si and O isotopes fractionate away from mantle-derived samples during low temperature water-rock interactions depending on the nature of the interaction (Robert and Chaussidon, 2006; Abraham et al, 2011; Wenner and Taylor, 1973; Muehlenbachs and Clayton, 1976). Trail et al. (2018) have shown that there could have existed reservoirs that were out of equilibrium with the mantle though investigation of zircons from S- I- A-type rocks, as well as detrital grains; in some cases, this inference was only reached because O isotopes and Si measurements were made simultaneously on the same zircons.

Given the long existence and the metamorphic history of the zircons measured here, their isotopic ratios might be disturbed but the measurements made here are considered valid because the O diffuses slowly enough during the cooling of the zircon such that the primordial isotopic characteristics of the crystal is preserved. While cooling, Watson and Cherniak (1997) suggests a closure temperature for O isotopes in zircon of ~650 °C for a cooling rate of 100 °C/Ma. This T is very close to the "wet" granite solidus and probably the T of formation for our zircons and thus the $^{18}O/^{16}O$ were probably locked-in soon after the zircon crystallized. But our samples have also experienced at least mid-amphibolite grade metamorphism which could have homogenized isotopic ratios. Cherniak and Watson, (2003), based on experiments performed by Watson and Cherniak, (1997), showed that at mid crustal temperatures of ~500 °C the core of the zircon will retain the primary $^{18}O/^{16}O$ ratio for a maximum of 0.1 Ga for a 20 µm core. This retention time will only increase for larger cores. More recent experimental studies have also posited that zircon cores can preserve $^{18}O/^{16}O$ ratios up to much higher metamorphic T of >800 °C (Bindeman et al., 2018). As for Si, the diffusivity of Si in zircon is at least five orders of magnitude slower compared to O under "wet" conditions at ~1000 °C and even slower under colder scenarios (Cherniak, 2008) so Si is likely preserved under most reasonable geologic conditions.

The zircons from the quartz-biotite schists (I370 and I374) show that the parent melt may have formed by re-melting of rocks that underwent hydration of primary silicates and authigenic silica precipitation. The datapoints that show a positive deviation in $\delta^{30}Si$ imply interaction with seawater (Trail et al., 2018) and authigenic silica formation that was re-melted to form the parent melt. Some recent work (André et al., 2019; Deng et al., 2019) shows that Archean granitoids could have evolved from melts that had significant proportions of chert-rich, silicified basalt, the presence of which could be explained by low-temperature water-rock interactions in the Hadean. The re-melting of such rock types suggests some sort of tectonic activity that contributed to the reworking of the rock record or an active silica cycle in the Eoarchean or earlier. Turner et al. (2014) propose a subduction like environment active during the time when the NSB was developing and it might be that the USB could have experienced similar environments but further geochemical analysis is required to prove this hypothesis.

In the modern age an active silica cycle is intricately linked to the long-term C cycle through silicate weathering (Walker et al., 1981; Edson et al., 2012). Silicate weathering contributes to the creation of silicate and carbonate-based microfossils. The absence of these organic Si sinks in the

Archean might have caused the precipitation of siliceous sediments as well as other inorganic components, which if re-melted at subduction zones, create reservoirs that are chemically distinct from the pristine mantle (Chen et al, 2020). Along with the inorganic siliceous components, the water-rock interactions mentioned above might have caused some of the alkali-rich minerals in the primary rocks to be chemically weathered to clay and mafic minerals to be serpentinized. This is reflected in the datapoints that show a negative and no deviation respectively in δ^{30}Si from the mantle values. The important thing to note here is that the δ^{30}Si values are, on average, in agreement with mantle-derived zircon, but the δ^{18}O values are mildly elevated from 'mantle' zircon values. The observations made here indicate two things, firstly, the parent melt might not be pristine mantle material and secondly, the parental melt for the zircons is consistent with having serpentinized lithologies and silicified basalts as significant components.

5.5 Zircon mineral Inclusions

The zircons from the quartz-biotite schists contain several primary inclusions that are isolated from cracks. The inclusions suite has a low abundance of apatite (13 ± 19 % 2 s.d.) and is dominated by quartz and feldspar indicating that the parent melt was probably felsic according to Bell et al. (2018). There are far more inclusions in contact with cracks than isolated inclusions. The former type of inclusions could imply that the zircons have experienced extensive volumes of hydrothermal fluids, since the quartz/feldspar ratio ($\frac{Quartz\ occurences}{(Feldspar\ occurences)}$) is higher in the on-crack category (1.4) than in the isolated category (0.75). This implies either that the infiltrating fluid was silica-saturated (and thus quartz was precipitated as secondary inclusions), or that primary inclusions were altered by the fluids, with feldspar being more susceptible. The fluid itself seems to be enriched in Fe, Al and Si since the crack-filling inclusions include biotite and other unidentified Fe-Al-Si rich phases. This is in-line with the observation made for some of the thin sections in which some feldspar phases are altered but biotite is relatively unscathed.

5.6 Protoliths for the quartz-biotite schists

When trying to establish the nature of the protolith that metamorphosed to form the quartz-biotite schists, comparisons need to be made with similar schists from the NSB. There is a general agreement that the NSB quartz-biotite schists are formed from detrital sediments (Cates and Mojzsis, 2007; Cates et al., 2013; David et al., 2009; Greer et al., 2020) and the USB schists might have a similar protolith given the textural, mineralogical and chemical similarities. The XRF analyses reveal that the parent melts for the rocks, that either supplied sediments for the schists or were the protoliths themselves, were granitic in terms of their chemistry and mineralogy. The Harker diagrams (**Fig. 11**) show that MgO, Fe_2O_3, Al_2O_3 and TiO_2 are negatively correlated with SiO_2. This implies that the NSB and the USB schists could have originated from the same magma source.

The mafic oxides mentioned have a lower concentration than the WS, which is an Archean mafic shale. The lower values imply that the USB schists had a more felsic progenitor compared to the WS. Furthermore, we see enrichments in Sr, depletions in Rb and especially Ni and Cr compared to the WS (**Fig. 12)**. **Fig. 12** also shows that the USB quartz-biotite schists are similar to the NSB schists and the MISB metasediments in terms of their chemistry. Cr/Th is a good indicator of the felsic nature of the melt (Condie and Wronkiewicz, 1990). Condie and Wronkiewicz, 1990, for instance, show that Archean granitoids have low Cr/Th (0.2 - 6.5) and Cr/Zr (0.04 – 0.3) values; the lower end being data from granites while the higher end is from tonalites. The same ratios have much higher values for basalts; 500 for the Cr/Th and 5.5 as goes the Cr/Zr. These diagnostic values were further verified by Gao et al. (1999) and Wu et al. (2012) when they measured gneisses from the Yangtse Craton, China. According to Gao et al. (1999), Cr/Th values are between 0.31 – 14.83 where the lower values are for granitic gneisses while the higher ones are for dioritic-trondjhemitic-tonalitic gneisses while the Cr/Zr values for the same lithologies are between 0.01 – 1.08.Wu et al. (2012) only measured tonalitic gneisses and their Cr/Th values are ~1.99 while the Cr/Zr values are ~0.1. These values are within range of the ones proposed by Condie and Wronkiewicz (1990). If the USB schists are derived from eroded granitoids, they should resemble them in terms of the two parameters just discussed. The USB schists analyzed here have Cr/Th values of 7.05 (I370) and 11.4 (I374) and Cr/Zr values of 0.22 (I370) and 0.39 (I374) which are close to the tonalitic values. Interestingly, the $\delta^{18}O$ values for the quartz-biotite schist zircons analyzed here is also similar to that of other Archean TTG zircons (Valley et al., 2005): ~5.53‰ (Barberton, South Africa) and 5.65 - 6.69‰ (Zircons from over 100,000 km^2 in the Superior Province).

For the NSB schists, there are large clasts of quartz and feldspar that might lead one to think that it is a metaconglomerate. The USB schists we have collected so far have no such clasts, but the zircons extracted from them are sub-rounded and not as euhedral (**Fig. S8**) as the gneissic zircons implying that they may have experienced erosion. MgO, Fe_2O_3, TiO_2 and MnO were plotted against Al_2O_3 for both the USB and the NSB schists. Except for TiO_2, which shows a strong correlation, all the other oxides show a weak to moderate correlation. This implies that the oxides are probably associated with clays and micas, the end-products of weathering and erosion, and not mafic minerals.

Finally, since most of the evidence indicate a sedimentary protolith, the rocks were compared on the classification diagram for sands and shales proposed by Herron (1988) along with NSB schists (**Fig. 13**). I374 plots in a location like most of the NSB schists while I370 plots in the “wacke” field, which might imply that I370 might be a bit more mature than the other schists and its protolith probably had a greater amount of feldspar grains or clays than the former. The major objective of using the classification diagram in Fig. 13 is to show how the major element measurements of similar lithologies from the NSB and the USB compare to each other and make careful and conservative inferences about the protoliths of the lithologies from the two belts. The classification diagram itself plays a secondary role and protolith inferences have to be a bit speculative since hydrothermal alteration might severely affect mobile oxides like K_2O but, most likely, both these belts could have undergone similar hydrothermal environments given their proximity which makes their intercomparison a valid exercise.

6. Conclusions

Integrated studies work to deconvolute multiple alterations and tectonic events that Eoarchean crustal enclaves have experienced, to finally distill the primary protolith of these enclaves. The main emphasis of the present study is the Ukaliq Supracrustal Belt in northern Québec, a large metamorphosed volcano-sedimentary enclave that may be structurally (and, petrogenetically) related to the neighboring Nuvvuagittuq Supracrustal Belt. Few studies have explored these rocks (Caro et al., 2017; Saji et al., 2018; Greer et al., 2020). Like the NSB, the USB is structurally complex and comprises medium to high grade metamorphosed rocks that have been hydrothermally altered. Physical and geochemical tests were done on these rocks to qualify the lithology of this belt, constrain out the ages of these rocks, understand whether the zircons analyzed for U-Pb geochronology were igneous or metamorphic, try and uncover what the protoliths of these rocks were and to establish similarities with the NSB. The major lithologies studied were schists, amphobolites, gneisses from the USB. We also followed up with additional thin section observation of a quartzite of controversial origin from the NSB. Thin section observations from all these rock types reveal that these rocks were not metasomatized uniformly and that even samples from the same rock unit display different alteration signatures. They also show that the USB rocks have experienced crystal-plastic deformation like the NSB.

Before analyzing the zircons extracted from these rock units, CL and BSE images were taken which show that all the zircons have igneous cores and some of them have rims of variable thicknesses. Subsequent care was taken to avoid these rims which will not provide information about the parent melts. Direct measurements have provided an Eoarchean age for the zircons extracted from the schists and the gneisses and show a tight cluster in their Th/U ratios suggesting that the measurements do not include metasomatized sections of the zircons. The ages of the gneisses and the quartz biotite schists (I370 and I374) are comparable to the NSB units of the same lithology and even to the Isua Supracrustal Belt. We propose that the gneisses have an emplacement age of 3.68 Ga and that the quartz-biotite schists have a maximum depositional age of 3.65 Ga. The depositional age of the USB schists is similar to the oldest ages of the zircons from the NSB schists. The melts from which they crystallized show that they possibly formed by the re-melting of either clay minerals, authigenic silica or serpentinized basalt or a mixture of some proportion containing some or all these materials although the last lithology seems to be most probable and a significant constituent. This implies that crustal processes such as chemical weathering that form clays and authigenesis as well as those that lead to re-melting of such lithologies were active during the Eoarchean/Hadean.

The probable nature of the protolith was further explored through major and trace element analysis of the quartz-biotite schists from the USB while being compared to similar lithologies from the NSB. The data suggests that the schists were metamorphosed products of detrital sediments. Zircons from the USB were also analyzed for their mineral inclusions and the Lu-Hf isotopic ratios. The mineral inclusion occurrences suggest that the parent melts were probably felsic. The Lu-Hf systematics also present a lot of chemical similarities between the USB and the NSB host rocks as well the constituent zircons implying a chemically similar source or the same source for both belts. Finally, based on the $\varepsilon_{Hf(t)}$ vs age plot for the USB and μNd^{142} anomalies reported for the USB and the NSB, the data are consistent with a Hadean reservoir that imparted its isotopic characteristic upon the mafic parent melt that was extracted at ~3.8 Ga. A significant observation we made is the similarity in U-Pb ages between the USB, NSB and the Isua Supracrustal Belt as well as the chemical similarity (Lu-Hf isotopes and Trace elements) between the quart-biotite schists of the USB and the NSB. These similarities might imply that these supracrustal belts could have been a larger single terrane or that these belts experienced similar geologic processes. This possibility was previously explored by Cates and Mojzsis (2007). Our study is an initial foray into establishing the geochemistry and thus the evolution of the USB which will be a step in the direction of studying the entire Inukjuak domain that might lend significant insight into the Hadean environment.

Acknowledgements

We thank Ming-Chang Liu for ion microprobe assistance. We also thank Ian Szumila and Yanling Wang for help with sample preparation. The field component of this work was supported by the Collaborative for Research in Origins (CRiO) at the University of Colorado Boulder, which is funded by the John Templeton Foundation-FfAME Origins program (S. Benner, PI); the opinions expressed in this publication are those of the authors, and do not necessarily reflect the views of the John Templeton Foundation. Support was also provided by NSF grants EAR-1545637, EAR-1650033, and the NASA PC_3 grant 80NSSC19M0069. The ion microprobe facility at UCLA is partially supported by a grant from the

Instrumentation and Facilities Program, Division of Earth Sciences, NSF grant EAR-1734856. Martin Guitreau acknowledges financial support from LabEx ClerVolc (ANR-10-LABX-0006), Région Auvergne, the European Regional Development Fund, and the French Agence Nationale de la Recherche (ANR) through the funded project *Zircontinents* (ANR-17-CE31-0021). Correspondence and request for materials should be addressed to Wriju Chowdhury (wchowdhu@ur.rochester.edu).

FIGURE CAPTIONS

Figure 1: Map showing the study area. The top left corner denotes the location of the town of Inukjuak. The red star designates all the sampling locations. The map inset (left) shows the general location of the field area which is on the eastern bank of the Hudson Bay. The inset maps show the location of the two supracrustal belts. The dotted square is the study area of Caro et al., (2017) while the solid square is the same for this study (Map modified from Caro et al., 2017). The vertical panel on the extreme right shows the samples collected. The GPS co-ordinates of all locations are listed in Table 1. Scale bar on the left inset map = 300 km and on the right inset map = 1 km.

F**igure. 2: a.** BSE (top four) and corresponding **b.** CL (bottom four) images of zircons from some of the gneisses mentioned in this study. Clockwise from the top left, the samples are I349, I349, I355 and I365 (Scale bars for both sets of images are 100µm). These zircons are representative of the gneissic zircons. Note the oscillatory zoning and the intact cores in all the zircons. The zircons contain cracks which were avoided during U-Pb analysis as best as possible. The circles (not to scale) show Laser ablation locations for U-Pb chronology and the corresponding ages are in Ga.

Figure 3: Zircons extracted from quartz-biotite schists of the USB. The images show BSE (Right panel) and corresponding CL (Left panel) from I370 (top set) and I374 (bottom set). These grains are representative of zircons from the schist. The grains show oscillatory zoning in the core; implying an igneous origin at least for the core. The grains also show prominent metamorphic rims that do not show any zoning and is uniform in its color. The circles show sputtering locations and the ages are ion microprobe Pb^{207}/Pb^{206} ages and Si and O stable isotope data. The scale bars in the left panel are 40 µm.

Figure 4: (a-d): Optical microscope pictures of the various rock types mentioned in this study. **(a)**. Quartz-biotite schist where the biotite is altered to chlorite. This is a sign of hydrothermal alteration in the USB much like the NSB. **(b).** Cummingtonite schist. Note the alterations on the basal sections. **(c)**. Biotite bearing gneiss. **(d)**. Fuchsite-bearing quartzite from the NSB. The fuchsite is the chaotic fibrolitic phase that appear as alterations. All images show evidence for hydrothermal alterations. **(e-f)**: **(e)**. Hornblende schist in the USB. This is one of the two kinds of amphibolites discussed in this study. The hornblende has been hydrothermally altered to chlorite crystallizing Fe/Ti-phases as a byproduct. **(f)**. Cummingtonite schist in the USB. The other kind of amphibolite which is found in both the USB and the NSB. The rock shows elongated and ribboned quartz grains implying that this sequence has experienced crystal-plastic deformation and subsequent relaxation as evidenced by the sub-grain formation. **(g-i)**: The two kinds of gneissic samples discussed in the work; Granitic gneiss **(g)** which is alkali-feldspar rich and tonalitic gneiss **(h)** which has significant plagioclase. Both gneisses are mica bearing and is commensurate with the general observation that the region has experienced amphibolite facies metamorphism. **(i)** the tonalitic gneiss also displays myrmekitic quartz (tubular quartz observed at the boundary between plagioclase and alkali feldspar). This kind of texture is observed as alkali feldspar is hydrothermally altered to plagioclase and the excess silica forms the observed tubular texture. There are also quartz grains that show ribboning and sub-grain formation which implies deformation and subsequent relaxation. Scale bar = 500 µm.

Figure 5: Clockwise from top left: I346, I349, I365, I355 Age histograms and corresponding Th/U of the zircons (All zircons analyzed and reported in Table **ST1b**) from some of the gneisses. The histograms all show a population at 3.4 Ga with some grains older at around 3.5 Ga. I349 has one grain at 3.71 ± 0.05 Ga but with a concordance of 109%. The large spread in Th/U values show that either there is a metamorphic component to the measurements or that the parent melt was not homogeneous. Most of the Th/U values of the youngest zircon analyses around 2.7 Ga are the lowest; this might be because of a metamorphic event around this time.

Figure 6: Clockwise from top left: I370, I374, IN05037, IN05020. Comparison of Age distributions of quartz-biotite schists zircons (Zircons reported in **Table ST1b**) from this study (two top figures; measured using an LA-ICP-MS) and from the same lithology in the NSB (two bottom figures; measured using a SIMS) (Cates and Mojzsis, 2007). The histograms show similar populations at 3.7 Ga and the oldest age of all the zircons analyzed is 3.79 Ga for the USB rock units. Th/U ratios in the USB are similar compared to the NSB Th/U values but have a smaller spread which may be because younger zircons were not analyzed.

Figure 7: Average ages and Th/U of the Core and Rim zones of zircons from gneiss samples of the USB. The ages of zones are similar for all samples except for I365. The Th/U ratio for I355 reduces from

the core to the rim indicating that the rim has a metamorphic component. Such trends are also observed for I346 although it is not as pronounced. The diamonds without an error bar have errors lower than the size of the diamond.

Figure 8: Si and O isotopic values of zircons from quartz-biotite schists of the USB (error bars are 2 s.e.). The datapoints in solid grey and white with grey borders are rejects because the sputtering pits hit cracks in the grain. The zircons show $\delta^{18}O$ values distinct from the mantle while the $\delta^{30}Si$ seems to be uniformly distributed about the mantle values.

Figure 9: A comparison of the $\delta^{30}Si$ against the age of zircons from the USB and the Jack Hills (Trail et al., 2018). In the case of multiple analyses of a sample, the average of all replicates has been plotted for the Jack Hills zircons. The USB zircons have the same average isotopic values as the Jack Hills zircons. One of the zircons having low $\delta^{30}Si$ has a $\delta^{18}O$ value quite close to mantle values implying that the zircon might be out of equilibrium with the mantle. Such evidences are also seen among the Jack Hills sample set.

Figure 10: Hf isotope signatures ($^{176}Hf/^{177}Hf$, ε_{Hf}) as a function of ages for zircons analyzed in this study (a-b) as well as zircons, granitoids and amphibolites from previous studies (c-d). CHUR values are from Iizuka et al., 2015). Grey dashed lines represent the evolution of geological reservoirs with $^{176}Lu/^{177}Hf$ of = 0.025 (basalt/gabbro), 0.006-0.002 (TTG; e.g., Guitreau et al., 2012), 0.002-0.0004 (zircon; this study). The good match between the datapoints and evolution lines for zircons (0.0004-0.002) in (a) and (b) suggests possible disturbances of the U-Pb isotope system resulting in younger ages than that of actual crystallization, no change in $^{176}Hf/^{177}Hf$, and spuriously low ε_{Hf} values. This evolution controlled by a very low $^{176}Lu/^{177}Hf$ is, however, not so different from that exhibited by magmatic zircon data as illustrated in (c) and (d). This general evolution line along a $^{176}Lu/^{177}Hf$ consistent with that of TTGs (e.g., Guitreau et al., 2012) is, hence, a true feature of NSB and USB, and echoes what can be seen in the Pietersburg block (South Africa; Laurent and Zeh, 2015).

Figure 11: The left and the center panel are Harker diagrams where the NSB and USB schists are shown together along with the Witswatersrand Shales (green triangles; Wronkiewicz and Condie, 1987), metasediments from the Isua supracrustal belt (yellow stars; Bolhar et al., 2005) and Archean platforms/shields (blue crosses; Rudnick and Fountain, 1995) . The mafic oxides, Al_2O_3, and P_2O_5 show negative correlations implying that the schists from the two belts formed by fractional crystallization from the same source. The K_2O values might be incorrect since the rocks are heavily altered. The absence of any trend in the alkali oxide plots however suggest that the rocks might be from different sources. The third panel shows that the mafic oxides are moderately to strongly correlated with Al_2O_3 suggesting that

the oxides might be associated with clays or micas rather than mafic minerals. (All concentration values are in percentages)

Figure 12: Trace element data for the USB Schists normalized to the NASC (North American Shale Composite). The green triangles are the average value from various shales from Witswatersrand, the yellow stars are the Isua metasediments and the blue crosses are Archean platforms/shields values. Note the similarities between the USB schists and the Archean lithologies. The USB schists are prominently depleted in Ni and Cr and enriched in Sr implying that the USB schist protoliths might be more felsic than the mafic shales or that the USB has been metasomatized which will cause a depletion in Ni and Cr. The other trace elements show broad similarities with the Archean shales implying that the USB schists could be metasediments. The grey band is the maximum and the minimum concentrations for each element across all the NSB quartz biotite schists analyzed by Cates et al. (2013).

Figure 13: The NSB (Cates et al., 2013 and Darling et al., 2013) and USB (This study) schists plotted on the classification diagram for sands and shales from Herron (1988). The USB and NSB schists seem to plot in similar locations. However, The K_2O values might be lower than from before the schists were hydrothermally altered which would put the unaltered rocks in a much more immature field. Isua metasediments (Bolhar et al., 2005) have also been shown for comparison.

TABLE CAPTIONS

Table 1: Details of samples collected for this study. GPS coordinates based on the WGS84 geodetic reference coordinate system.

Table 2: ^{207}Pb/^{206}Pb ages reported in the manuscript. The ages considered here are derived for zircons that are between 90 and 100% concordant. The errors are 2 standard deviation. For I373, the U-Pb date has been reported from analyses made in the intermediate region between the core and the rim.

SUPPLEMENTARY INFORMATION

SUPPLEMENTARY FIGURE CAPTIONS

Figure S1: a. Continuous schistosity defined by the mafic and felsic minerals of the rock. Note the extensive alteration of the biotite to chlorite. This is probably caused by a K and Fe deficient fluids. **b, c.** Other biotite schists showing minimal alteration of the biotite **(b)** and moderate alteration **(c)**. The dark spots on the biotite crystals are radiation haloes caused by radioactive inclusions. The study area is characterized by samples from the same rock unit showing signs of having been affected differently by hydrothermal fluids. Scale bar = 500 µm. **d.** Quartz grains from gneisses showing grain boundary migration and sub grain formation. Note the triple junction between quartz grains implying growth or an alteration of the grain boundary during a metamorphic event. Scale bar = 200 µm. **e.** Possible matrix inclusion in quartz. These finer grains might have been captured during growth of the quartz grains during a metamorphic event. The quartz grains also show a triangular grain boundary which is another sign that there was growth during a thermal event. Scale bar = 100 µm. **f.** Hornblende schist from the USB. This section shows quartz porphyroblasts (not surrounded by fine-grained matrix) with biotite crystals flowing around the grains (encircled). This observation is unique to this thin section. Such textures might mean that these quartz grains grew during a deformation event rather than being a primordial igneous grain. Scale bar = 500 µm. (Images in Plane polarized light using an Optical Microscope). **g-i.** Field photographs of some of the gneisses sampled. **j-l.** The quartz-biotite schists discussed in the text. The red circle in photo **l** shows the coin we used for scale. Note the alterations and weathering on all the rocks. Abbreviations: QBS – Quartz-biotite Schists, Gn – Gneiss. Hammer and coin used for scale.

Figure S2: **a.** Relatively clean plagioclase and altered biotite: probably K-deficient fluid; since biotite altered to chlorite involves K^+ being removed from the biotite crystal structure and the Fe being re-arranged to form chlorite grains. Al can also be added during chloritization. **b.** Altered plagioclase (smudged colorless phase) with relatively unaltered biotite: K and Fe-saturated fluid; since plagioclase being altered to K-rich clay is an indicator of a K-rich fluid. Also, since it is observed that biotite is not as altered as the section on the left, the same conclusion about fluid chemistry may be reached. Scale bars = 500 µm. (Plane polarized light). **c.** Plagioclase surrounding relict K-feldspar grain in the purported Tonalitic gneiss. This rock may have been granitic to begin with and the alkali feldspar might have been altered to plagioclase. Or the K-feldspar may be secondary and formed after the plagioclase was affected by a K-rich fluid from which the K-feldspar crystallized. **d.** Minor plagioclase occurrences in the fuchsite bearing quartzite. Scale bar = 500 µm. (Cross-Polarized light (XPL)).

Figure S3: The zircon grains from **(a)** orthogneisses and **(b)** quartz-biotite schists that have been considered when presenting ages for the units. Note that the I373 grains are analyses from an intermediate region of the zircon. The green triangles are age markers. All ratios reported here were measured using an LA-ICP-MS.

Figure S4: Comparison of Pb^{207}/Pb^{206} average ages measured on zircons from the quartz-biotite schist of the USB. The SIMS measurements are more precise than the LA-ICP-MS measurements in this study. All measurements used to calculate this average age has % concordance between 90 and 100. The data has been listed in Table 2.

Figure S5: Age distributions and Th/U ratios of unconsolidated sediments collected from stream beds. All distributions show a strong peak at ~2.7 Ga which is mostly because the surrounding igneous suite dominates the regional lithology. The younger zircons have a large range of Th/U ratios implying that igneous activity was coeval with a metamorphic event.

Figure S6: Secondary electron image of a chromite grain surrounded by fuchsite from the NSB. The texture of the grain suggests dissolution of the spinel to form the Cr-rich mica. The mica might therefore be a secondary deposit. (Image taken using a Zeiss Auriga SEM/FIB at the University of Rochester).

Figure S7: CL image of zircon grain I370_3_7 whose laser ablation age was selected as the maximum depositional age for the quartz-biotite-schists. The prominent oscillatory zoning shows that the core of the zircon is magmatic in origin.

Figure S8: BSE (Top) and CL (Bottom) images of representative zircons from the USB Quartz-biotite schist. These zircons are sub-rounded and not as euhedral as the gneissic zircons implying that these zircons underwent transport. Scale bars = 10 µm.

SUPPLEMENTARY TABLE CAPTIONS

Table ST1: a. Instrumental Parameters for U-Pb geochronology using an LA-ICP-MS**. b.** Results of the U-Pb geochronology on detrital zircon grains using an LA-ICP-MS. **c.** Results of the U-Pb geochronology on detrital zircon grains using a SIMS.

Table ST2: Results of the U-Pb geochronology on detrital zircon grains from the unconsolidated sediments using an LA-ICP-MS.

Table ST3: Parameters for the Lu-Hf measurements.

Table ST4: Results of the Si and O isotope measurements on the detrital zircons.

Table ST5: Results of the mineral inclusion study of the detrital zircons.

Table ST6: Raw data for the Si and O measurements

Table ST7: Results for the Lu-Hf measurements.

Table ST8: Major and trace element values of the whole rock measurements performed on the quartz-biotite schists.

REFERENCES

Abraham, K., A. Hofmann, S. F. Foley, D. Cardinal, C. Harris, M. G. Barth and L. Andre (2011). "Coupled silicon-oxygen isotope fractionation traces Archaean silicification." Earth and Planetary Science Letters **301**(1-2): 222-230.

Adam, J., T. Rushmer, J. O'Neil and D. Francis (2012). "Hadean greenstones from the Nuvvuagittuq fold belt and the origin of the Earth's early continental crust." Geology **40**(4): 363-366.

André, L., K. Abraham, A. Hofmann, L. Monin, I. C. Kleinhanns and S. Foley (2019). "Early continental crust generated by reworking of basalts variably silicified by seawater." Nature Geoscience **12**(9): 769.

Augland, L. E. and J. David (2015). "Protocrustal evolution of the Nuvvuagittuq Supracrustal Belt as determined by high precision zircon Lu-Hf and U-Pb isotope data." Earth and Planetary Science Letters **428**: 162-171.

Basilevsky, A. T. and J. W. Head (2002). "Venus: Timing and rates of geologic activity." Geology **30**(11): 1015-1018.

Bauer, A. M., C. M. Fisher, J. D. Vervoort and S. A. Bowring (2017). "Coupled zircon Lu-Hf and U-Pb isotopic analyses of the oldest terrestrial crust, the > 4.03 Ga Acasta Gneiss Complex." Earth and Planetary Science Letters **458**: 37-48.

Bédard, J. H., et al (2003). "Archaean cratonization and deformation in the northern Superior Province, Canada: an evaluation of plate tectonic versus vertical tectonic models." Precambrian Research **127**(1-3): 61-87.

Bell, E. A., P. Boehnke, M. D. Hopkins-Wielicki and T. M. Harrison (2015). "Distinguishing primary and secondary inclusion assemblages in Jack Hills zircons." Lithos 234: 15-26.

Bell, E. A. (2016). "Preservation of primary mineral inclusions and secondary mineralization in igneous zircon: a case study in orthogneiss from the Blue Ridge, Virginia." Contributions to Mineralogy and Petrology 171(3).

Bell, E. A., et al. (2017). "Applications of biotite inclusion composition to zircon provenance determination." Earth and Planetary Science Letters **473**: 237-246.

Bell, E. A., P. Boehnke, T. M. Harrison and M. M. Wielicki (2018). "Mineral inclusion assemblage and detrital zircon provenance." Chemical Geology 477: 151-160.

Bindeman, I. N., A. K. Schmitt, C. C. Lundstrom and R. L. Hervig (2018). "Stability of Zircon and Its

Isotopic Ratios in High-Temperature Fluids: Long-Term (4 months) Isotope Exchange Experiment at 850 degrees C and 50 MPa." Frontiers in Earth Science **6**(59).

Blichert-Toft, J. (2008). "The Hf isotopic composition of zircon reference material 91500." Chemical Geology **253**(3-4): 252-257.

Blichert-Toft, J., S. J. Mojzsis, L. Cates N, G. Caron, D. Trail, O. Abramov, M. Guitreau, W. M. D. Hopkins and W. Bleeker (2014). "Component geochronology in the polyphase ca. 3920 Ma Acasta Gneiss." Geochimica et Cosmochimica Acta **133**: 68-96.

Boehnke, P., E. A. Bell, T. Stephan, R. Trappitsch, C. B. Keller, O. S. Pardo, A. M. Davis, T. M. Harrison and M. J. Pellin (2018). "Potassic, high-silica Hadean crust." Proceedings of the National Academy of Sciences of the United States of America **115**(25): 6353-6356.

Bolhar, R., B. S. Kamber, S. Moorbath, M. J. Whitehouse and K. D. Collerson (2005). “Chemical characterization of earth's most ancient clastic metasediments from the Isua Greenstone Belt, southern West Greenland.” Geochimica et Cosmochimica Acta **69:** 1555.

Bourdon, B. and G. Caro (2007). "The early terrestrial crust." Comptes Rendus Geoscience **339**(14-15): 928-936.

Bowring, S. A. and I. S. Williams (1999). "Priscoan (4.00-4.03 Ga) orthogneisses from northwestern Canada." Contributions to Mineralogy and Petrology **134**(1): 3-16.

Boyet, M., et al. (2003). "Nd-142 evidence for early Earth differentiation." Earth and Planetary Science Letters **214**(3-4): 427-442.

Boyet, M. and R. W. Carlson (2005). "Nd-142 evidence for early (> 4.53 Ga) global differentiation of the silicate Earth." Science **309**(5734): 576-581.

Bridgwater D, McGregor VR (1974). “Field work on the very early Precambrian rocks of the Isua area, Southern West Greenland.” Rapp Gronlands Geol Unders **65**:49-53.

Caro, G., et al. (2003). "Sm-146-Nd-142 evidence from Isua metamorphosed sediments for early differentiation of the Earth's mantle." Nature **423**(6938): 428-432.

Caro, G., et al. (2005). "Trace-element fractionation in Hadean mantle generated by melt segregation from a magma ocean." Nature **436**(7048): 246-249.

Caro, G., et al. (2017). "Sluggish Hadean geodynamics: Evidence from coupled ^{146,147}Sm-^{142,143}Nd systematics in Eoarchean supracrustal rocks of the Inukjuak domain (Québec)." Earth and Planetary

Science Letters **457**: 23-37.

Cates, N. L. and S. J. Mojzsis (2006). "Chemical and isotopic evidence for widespread Eoarchean metasedimentary enclaves in southern West Greenland." Geochimica Et Cosmochimica Acta **70**(16): 4229-4257.

Cates, N. L. and S. J. Mojzsis (2007). "Pre-3750 Ma supracrustal rocks from the Nuvvuagittuq supracrustal belt, northern Québec." Earth and Planetary Science Letters **255**(1-2): 9-21.

Cates, N. L. and S. J. Mojzsis (2009). "Metamorphic zircon, trace elements and Neoarchean metamorphism in the ca. 3.75 Ga Nuvvuagittuq supracrustal belt, Québec (Canada)." Chemical Geology **261**(1-2): 98-113.

Cates, N. L., et al. (2013). "Reduced, reused and recycled: Detrital zircons define a maximum age for the Eoarchean (ca. 3750-3780 Ma) Nuvvuagittuq Supracrustal Belt, Québec (Canada)." Earth and Planetary Science Letters **362**: 283-293.

Cavosie, A. J., J. W. Valley, S. A. Wilde and E.I.M.F (2005). "Magmatic δ18O in 4400–3900 Ma detrital zircons: A record of the alteration and recycling of crust in the Early Archean." Earth and Planetary Science Letters **235**(3-4): 663-681.

Chen, AX., Li, YH., Chen, Y., Yu, HM., Huang, F. (2020). “Silicon isotope composition of subduction zone fluids as recorded by Jadeitites from Myanmar.” Contributions to Mineralogy and Petrology **175**: 6.

Cherniak, D. J. and E. B. Watson (2003). Diffusion in zircon. Zircon. J. M. Hanchar and P. W. O. Hoskin. **53:** 113-143.

Cherniak, D. J. (2008). "Si diffusion in zircon." Physics and Chemistry of Minerals **35**(4): 179-187.

Compston, W. and R. T. Pidgeon (1986). "Jack Hills, Evidence of More Very Old Detrital Zircons in Western-Australia." Nature **321**(6072): 766-769.

Condie, K. C., (2019). “Earth’s Oldest Rocks and Minerals.” Earth’s Oldest Rocks **Chapter 11**:239 Pub:Elsevier.

Condie, K. C. and D. J. Wronkiewicz (1990). "The Cr/Th Ratio in Precambrian Pelites from the Kaapvaal Craton as an Index of Craton Evolution." Earth and Planetary Science Letters **97**(3-4): 256-267.

Darling, J. R., et al. (2013). “Eoarchean to Neoarchean evolution of the Nuvvuagittuq Supracrustal Belt: New insights from U-Pb zircon Geochronology.” American Journal of Science **313:** 844-876.

Dauphas, N., et al. (2007). "Identification of chemical sedimentary protoliths using iron isotopes in the > 3750 Ma Nuvvuagittuq supracrustal belt, Canada." Earth and Planetary Science Letters **254**(3-4): 358-376.

David, J., et al. (2009). “U-Pb ages (3.8–2.7 Ga) and Nd isotope data from the newly identified Eoarchean Nuvvuagittuq supracrustal belt, superior Craton, Canada.” Geol Soc Am Bull **121**(1–2):150–163.

Deng, Z. B., M. Chaussidon, M. Guitreau, I. S. Puchtel, N. Dauphas and F. Moynier (2019). "An oceanic subduction origin for Archaean granitoids revealed by silicon isotopes." Nature Geoscience **12**(9): 774.

Dodd, M. S., D. Papineau, T. Grenne, J. F. Slack, M. Rittner, F. Pirajno, J. O'Neil and C. T. S. Little (2017). "Evidence for early life in Earth's oldest hydrothermal vent precipitates." Nature **543**(7643): 60.

Edson, A. R., J. F. Kasting, D. Pollard, S. Lee and P. R. Bannon (2012). "The Carbonate-Silicate Cycle and CO2/Climate Feedbacks on Tidally Locked Terrestrial Planets." Astrobiology **12**(6): 562-571.

Fisher, C. M., J. M. Hanchar, S. D. Samson, B. Dhuime, J. Blichert-Toft, J. D. Vervoort and R. Lam (2011). "Synthetic zircon doped with hafnium and rare earth elements: A reference material for in situ hafnium isotope analysis." Chemical Geology **286**(1-2): 32-47.

Fisher, C. M., J. D. Vervoort and J. M. Hanchar (2014). "Guidelines for reporting zircon Hf isotopic data by LA-MC-ICPMS and potential pitfalls in the interpretation of these data." Chemical Geology **363**: 125-133.

Foley, B. J. and H. Rizo (2017). “Long-term preservation of early formed mantle heterogeneity by mobile lid convection: Importance of grainsize evolution” Earth and Planetary Science Letters **475:** 94-105.

Froude, D. O., T. R. Ireland, P. D. Kinny, I. S. Williams, W. Compston, I. R. Williams and J. S. Myers (1983). "Ion microprobe identification of 4,100–4,200 Myr-old terrestrial zircons." Nature **304**(5927): 616-618.

Furnes, H., M. d. Wit, H. Staudigel, M. Rosing and K. Muehlenbachs (2007). “A Vestige of Earth's Oldest Ophiolite. United States.” Science **315:** 1704-1707.

Ickert, R. B. (2013). "Algorithms for estimating uncertainties in initial radiogenic isotope ratios and model ages." Chemical Geology **340**: 131-138.

Foley, B. J., et al. (2014). "Initiation of plate tectonics from post-magma ocean thermochemical convection." Journal of Geophysical Research-Solid Earth **119**(11): 8538-8561.

Gao, S., W. Ling, Y. Qiu, Z. Lian, G. Hartmann and K. Simon (1999). “Contrasting geochemical and Sm-Nd isotopic compositions of Archean metasediments from the Kongling high-grade terrain of the Yangtze craton: evidence for cratonic evolution and redistribution of REE during crustal anatexis.” Geochimica et Cosmochimica Acta **63:** 2071-2088.

Gerdes, A. and A. Zeh (2009). "Zircon formation versus zircon alteration - New insights from combined U-Pb and Lu-Hf in-situ LA-ICP-MS analyses, and consequences for the interpretation of Archean zircon from the Central Zone of the Limpopo Belt." Chemical Geology **261**(3-4): 230-243.

Greer, J., G. Caro, N. L. Cates, P. Tropper, W. Bleeker, N. M. Kelly and S. J. Mojzsis (2020). “Widespread poly-metamorphosed Archean granitoid gneisses and supracrustal enclaves of the southern Inukjuak Domain, Québec (Canada).” Lithos. **364-365:** 105520.

Griffin, W. L., E. A. Belousova, C. O'Neill, S. Y. O'Reilly, V. Malkovets, N. J. Pearson, S. Spetsius and S. A. Wilde (2014). “The world turns over: Hadean–Archean crust–mantle evolution.” Lithos **189:** 2-15.

Gromet, L. P., R. F. Dymek, L. A. Haskin and R. L. Korotev (1984). "The North-American Shale Composite - Its Compilation, Major and Trace-Element Characteristics." Geochimica Et Cosmochimica Acta **48**(12): 2469-2482.

Guitreau, M., J. Blichert-Toft, H. Martin, S. J. Mojzsis and F. Albarede (2012). "Hafnium isotope evidence from Archean granitic rocks for deep-mantle origin of continental crust." Earth and Planetary Science Letters **337**: 211-223.

Guitreau, M., et al. (2013). "A legacy of Hadean silicate differentiation inferred from Hf isotopes in Eoarchean rocks of the Nuvvuagittuq supracrustal belt (Québec, Canada)." Earth and Planetary Science Letters **362**: 171-181.

Guitreau, M. and J. Blichert-Toft (2014). "Implications of discordant U-Pb ages on Hf isotope studies of detrital zircons." Chemical Geology **385**: 17-25.

Harrison, T. M., A. K. Schmitt, M. T. McCulloch and O. M. Lovera (2008). "Early (>= 4.5 Ga) formation of terrestrial crust: Lu-Hf, delta O-18, and Ti thermometry results for Hadean zircons." Earth and Planetary Science Letters **268**(3-4): 476-486.

Harrison, T. M., et al. (2017). "Hadean Zircon Petrochronology: Petrochronology: Methods and Applications” Reviews in Mineralogy and Geochemistry (2017) **83**(1): 329-363.

Herron, M. M., (1988). “Geochemical classification of terrigenous sands and shales from core or log data.” Journal of Sedimentary Research **58** (5): 820–829.

Iizuka, T., T. Yamaguchi, Y. Hibiya and Y. Amelin (2015). "Meteorite zircon constraints on the bulk Lu-Hf isotope composition and early differentiation of the Earth." Proceedings of the National Academy of Sciences of the United States of America **112**(17): 5331-5336.

Jacobson, S. A., D. C. Rubie, J. Hernlund, A. Morbidelli and M. Nakajima (2017). "Formation, stratification, and mixing of the cores of Earth and Venus." Earth and Planetary Science Letters **474**: 375-386.

Jagoutz, O. and M. D. Behn (2013). "Foundering of lower island-arc crust as an explanation for the origin of the continental Moho." Nature **504**(7478): 131.

King, S. D. (2005). "Archean cratons and mantle dynamics." Earth and Planetary Science Letters **234**(1-2): 1-14.

Kirkland, C. L., R. H. Smithies, R. J. M. Taylor, N. Evans and B. McDonald (2015). "Zircon Th/U ratios in magmatic environs." Lithos **212**: 397-414.

Korenaga, J. (2006). "Archean geodynarnics and the thermal evolution of earth." Archean Geodynamics and Environments **164**: 7-32.

Korenaga, J. (2018). “Crustal evolution and mantle dynamics through Earth history.” Philosophical Transactions of the Royal Society A **376:** 20170408.

Laurent, O. and A. Zeh (2015). "A linear Hf isotope-age array despite different granitoid sources and complex Archean geodynamics: Example from the Pietersburg block (South Africa)." Earth and Planetary Science Letters **430**: 326-338.

Maier, A. C., N. L. Cates, D. Trail and S. J. Mojzsis (2012). "Geology, age and field relations of Hadean zircon-bearing supracrustal rocks from Quad Creek, eastern Beartooth Mountains (Montana and Wyoming, USA)." Chemical Geology **312**: 47-57.

Manning, C. E., S. J. Mojzsis and T. M. Harrison (2006). "Geology, Age and Origin of Supracrustal Rocks at Akilia, West Greenland." American Journal of Science **306**(5): 303-366.

Martin, H., J. F. Moyen, M. Guitreau, J. Blichert-Toft and J. L. Le Pennec (2014). "Why Archaean TTG cannot be generated by MORB melting in subduction zones." Lithos **198**: 1-13.

Mloszewska, A. M., E. Pecoits, N. L. Cates, S. J. Mojzsis, J. O'Neil, L. J. Robbins and K. O. Konhauser (2012). "The composition of Earth's oldest iron formations: The Nuvvuagittuq Supracrustal Belt (Québec, Canada)." Earth and Planetary Science Letters **317**: 331-342.

Mloszewska, A. M., S. J. Mojzsis, E. Pecoits, D. Papineau, N. Dauphas and K. O. Konhauser (2013). "Chemical sedimentary protoliths in the > 3.75 Ga Nuvvuagittuq Supracrustal Belt (Québec, Canada)." Gondwana Research **23**(2): 574-594.

Moorbath, S., et al. (1973). "Early Archaean Age for Isua Iron Formation, West Greenland." Nature **245**(5421): 138-139.

Mojzsis, S. J. and T. M. Harrison (2002). "Establishment of a 3.83-Ga magmatic age for the Akilia tonalite (southern West Greenland)." Earth and Planetary Science Letters **202**(3-4): 563-576.

Mojzsis, S. J., et al. (2019). "Onset of giant planet migration before 4480 million years ago." The Astrophysical Journal **881**(44): 13pp.

Moyen, J. F. and H. Martin (2012). "Forty years of TTG research." Lithos **148**: 312-336.

Muehlenbachs, K. and R. N. Clayton (1976). "Oxygen Isotope Composition of Oceanic-Crust and Its Bearing on Seawater." Journal of Geophysical Research **81**(23): 4365-4369.

Nakajima, M. and D. J. Stevenson (2015). "Melting and mixing states of the Earth's mantle after the Moon-forming impact." Earth and Planetary Science Letters **427**: 286-295.

Nutman, A. P., et al. (1996). "The Itsaq Gneiss Complex of southern west Greenland; The world's most extensive record of early crustal evolution (3900-3600 Ma)." Precambrian Research **78**(1-3): 1-39.

Nutman, A. P., C. R. L. Friend, S. L. L. Barker and V. R. McGregor (2004). "Inventory and assessment of Palaeoarchaean gneiss terrains and detrital zircons in southern West Greenland." Precambrian Research **135**(4): 281-314.

Nutman, A. P., R. Maciejowski and Y. S. Wan (2014). "Protoliths of enigmatic Archaean gneisses established from zircon inclusion studies: Case study of the Caozhuang quartzite, E. Hebei, China." Geoscience Frontiers **5**(4): 445-455.

O'Neil, J., C. Maurice, R. K. Stevenson, J. Larocque, C. Cloquet, J. David and D. Francis (2007). "The Geology of the 3.8 Ga Nuvvuagittuq (Porpoise Cove) Greenstone Belt, Northeastern Superior Province, Canada." Earth's Oldest Rocks **15**: 219-250.

O'Neil, J., et al. (2008). "Neodymium-142 evidence for hadean mafic crust." Science **321**(5897): 1828-1831.

O'Neil, J., et al. (2012). "Formation age and metamorphic history of the Nuvvuagittuq Greenstone Belt." Precambrian Research **220**: 23-44.

O'Neil, J., M. Boyet, R. W. Carlson and J. L. Paquette (2013). "Half a billion years of reworking of Hadean mafic crust to produce the Nuvvuagittuq Eoarchean felsic crust." Earth and Planetary Science Letters **379**: 13-25.

O'Neil J., Rizo H., Boyet M., Carlson R.W., Rosing M.T. (2016). “Geochemistry and Nd isotopic characteristics of Earth's Hadean mantle and primitive crust.” Earth and Planetary Science Letters **442**:194-205.

O'Neil J. and Carlson R.W (2017). “Building Archean cratons from Hadean mafic crust.” Science **355**(6330):1199-202.

O'Neill, C. and V. Debaille (2014). "The evolution of Hadean-Eoarchaean geodynamics." Earth and Planetary Science Letters **406**: 49-58.

Paces, J. B. and J. D. Miller (1993). "Precise U-Pb Ages of Duluth Complex and Related Mafic Intrusions, Northeastern Minnesota - Geochronological Insights to Physical, Petrogenetic, Paleomagnetic, and Tectonomagmatic Processes Associated with the 1.1 Ga Midcontinent Rift System." Journal of Geophysical Research-Solid Earth **98**(B8): 13997-14013.

Patchett, P. J. (1983). "Importance of the Lu-Hf Isotopic System in Studies of Planetary Chronology and Chemical Evolution." Geochimica Et Cosmochimica Acta **47**(1): 81-91.

Paton, C., J. Hellstrom, B. Paul, J. Woodhead and J. Hergt (2011). "Iolite: Freeware for the visualisation and processing of mass spectrometric data." Journal of Analytical Atomic Spectrometry **26**(12): 2508-2518.

Peck, W. H., J. W. Valley, S. A. Wilde and C. M. Graham (2001). "Oxygen isotope ratios and rare earth elements in 3.3 to 4.4 Ga zircons: Ion microprobe evidence for high delta O-18 continental crust and oceans in the Early Archean." Geochimica Et Cosmochimica Acta **65**(22): 4215-4229.

Polat, A., A. W. Hofmann and M. T. Rosing (2002). “Boninite-like volcanic rocks in the 3.7–3.8 Ga Isua greenstone belt, West Greenland: geochemical evidence for intra-oceanic subduction zone processes in the early Earth.” Chemical Geology **184:** 231-254.

Quidelleur, X., M. Grove, O. M. Lovera, T. M. Harrison, A. Yin and F. J. Ryerson (1997). "Thermal evolution and slip history of the Renbu Zedong Thrust, southeasterm Tibet." Journal of Geophysical Research-Solid Earth **102**(B2): 2659-2679.

Rapp, R. P. and E. B. Watson (1995). "Dehydration Melting of Metabasalt at 8-32-Kbar - Implications for Continental Growth and Crust-Mantle Recycling." Journal of Petrology **36**(4): 891-931.

Raza, M., V. R. Bhardwaj, A. H. M. Ahmad, M. E. A. Mondal, A. Khan and M. S. Khan (2010). "Provenance and weathering history of Archaean Naharmagra quartzite of Aravalli craton, NW Indian shield: Petrographic and geochemical evidence." Geochemical Journal **44**(5): 331-345.

Reimink, J. R., T. Chacko, R. W. Carlson, S. B. Shirey, J. A. Liu, R. A. Stern, A. M. Bauer, D. G. Pearson and L. M. Heaman (2018). "Petrogenesis and tectonics of the Acasta Gneiss Complex derived from integrated petrology and Nd-142 and W-182 extinct nuclide-geochemistry." Earth and Planetary Science Letters **494**: 12-22.

Rizo, H., et al. (2011). "Combined Nd and Hf isotope evidence for deep-seated source of Isua lavas." Earth and Planetary Science Letters **312**(3-4): 267-279.

Robin, C. M. I. and R. C. Bailey (2009). "Simultaneous generation of Archean crust and subcratonic roots by vertical tectonics." Geology **37**(6): 523-526.

Robert, F. and M. Chaussidon (2006). "A palaeotemperature curve for the Precambrian oceans based on silicon isotopes in cherts." Nature **443**(7114): 969-972.

Rolf, T., B. Steinberger, U. Sruthi and S. C. Werner (2018). "Inferences on the mantle viscosity structure and the post-overturn evolutionary state of Venus." Icarus **313**: 107-123.

Roth, A. S. G., et al. (2013). "Inherited Nd-142 anomalies in Eoarchean protoliths." Earth and Planetary Science Letters **361**: 50-57.

Rubatto, D. (2002). "Zircon trace element geochemistry: partitioning with garnet and the link between U–Pb ages and metamorphism." Chemical Geology **184**(1): 123-138.

Rudnick, R. L. and D. M. Fountain (1995). “Nature and composition of the continental crust: A lower crustal perspective.” Reviews of Geophysics **33:** 267-309.

Sañudo-Wilhelmy, S. A. and A. R. Flegal (1994). "Temporal variations in lead concentrations and isotopic composition in the Southern California Bight." Geochimica et Cosmochimica Acta **58**(15): 3315-3320.

Saji, N. S., et al. (2018). "Hadean geodynamics inferred from time-varying Nd-142/Nd-144 in the early Earth rock record." Geochemical Perspectives Letters **7**: 43-48.

Scherer, E., C. Munker and K. Mezger (2001). "Calibration of the lutetium-hafnium clock." Science **293**(5530): 683-687.

Schmitt, A. K. and J. A. Vazquez (2017). "Secondary Ionization Mass Spectrometry Analysis in

Petrochronology." Petrochronology: Methods and Applications **83**: 199.

Shirey, S. B. and S. H. Richardson (2011). "Start of the Wilson Cycle at 3 Ga Shown by Diamonds from Subcontinental Mantle." Science **333**(6041): 434-436.

Simard, M., Parent, M., David, J. and Sharma, K. N. M. (2003). “Géologie de la région de la rivière Innuksuac (34K et 34L).” Ministère des Ressources naturelles, Québec; **RG 2002-10**: 46 pages.

Sleep, N. H., K. J. Zahnle and R. E. Lupu (2014). "Terrestrial aftermath of the Moon-forming impact." Philosophical transactions. Series A, Mathematical, physical, and engineering sciences **372**(2024): 20130172.

Söderlund, U., P. J. Patchett, J. D. Vervoort and C. E. Isachsen (2004). "The 176Lu decay constant determined by Lu–Hf and U–Pb isotope systematics of Precambrian mafic intrusions." Earth and Planetary Science Letters **219**(3-4): 311-324.

Stevenson, R. K. and P. J. Patchett (1990). "Implications for the Evolution of Continental-Crust from Hf-Isotope Systematics of Archean Detrital Zircons." Geochimica Et Cosmochimica Acta **54**(6): 1683-1697.

Thomassot, E., J. O'Neil, D. Francis, P. Cartigny and B. A. Wing (2015). "Atmospheric record in the Hadean Eon from multiple sulfur isotope measurements in Nuvvuagittuq Greenstone Belt (Nunavik, Québec)." Proceedings of the National Academy of Sciences of the United States of America **112**(3): 707-712.

Tonks, W. B. and H. J. Melosh (1993). "Magma Ocean Formation Due to Giant Impacts." Journal of Geophysical Research-Planets **98**(E3): 5319-5333.

Trail, D., et al. (2018). "Origin and significance of Si and O isotope heterogeneities in Phanerozoic, Archean, and Hadean zircon." Proceeding of the National Academy of Sciences **115**(41): 10287-10292.

Trail, D., et al. (2016). "Li zoning in zircon as a potential geospeedometer and peak temperature indicator." Contributions to Mineralogy and Petrology **171**(3).

Trail, D., et al. (2017). "Aluminum in zircon as evidence for peraluminous and metaluminous melts from the Hadean to present." Geochemistry Geophysics Geosystems **18**(4): 1580-1593.

van Thienen, P., et al. (2004). "Production and recycling of oceanic crust in the early Earth." Tectonophysics **386**(1-2): 41-65.

Turner, S., T. Rushmer, M. Reagan and J. F. Moyen (2014). “Heading down early on? Start of subduction on Earth.” Geology **42**(2)**:** 139-142.

Turner, S., Wilde, S., Wörner, G., Schaefer, B., Lai, Y.J. (2020). “An andesitic source for Jack Hills zircon supports onset of plate tectonics in the Hadean.” Nature Communications **11**:1241

Valley, J. W., J. S. Lackey, A. J. Cavosie, C. C. Clechenko, M. J. Spicuzza, M. A. S. Basei, I. N. Bindeman, V. P. Ferreira, A. N. Sial, E. M. King, W. H. Peck, A. K. Sinha and C. S. Wei (2005). “4.4 billion years of crustal maturation: oxygen isotope ratios of magmatic zircon.” Contributions to Mineralogy and Petrology **150:** 561-580.

Vervoort, J. D., P. J. Patchett, U. Soderlund and M. Baker (2004). "Isotopic composition of Yb and the determination of Lu concentrations and Lu/Hf ratios by isotope dilution using MC-ICPMS." Geochemistry Geophysics Geosystems **5**:1-15.

Walker, J. C. G., P. B. Hays and J. F. Kasting (1981). "A negative feedback mechanism for the long term stabilization of Earth’s surface temperature.” Journal of Geophysical Research-Oceans **86**(NC10): 9776-9782.

Watson, E. B. and D. J. Cherniak (1997). "Oxygen diffusion in zircon." Earth and Planetary Science Letters **148**(3-4): 527-544.

Weiss, B. P., et al. (2018). "Secondary magnetic inclusions in detrital zircons from the Jack Hills, Western Australia, and implications for the origin of the geodynamo." Geology **46**(5): 427-430.

Woodhead, J. D. and J. M. Hergt (2005). "A preliminary appraisal of seven natural zircon reference materials for in situ Hf isotope determination." Geostandards and Geoanalytical Research **29**(2): 183-195.

Wenner, D. B. and H. P. Taylor (1973). "Oxygen and Hydrogen Isotope Studies of Serpentinization of Ultramafic Rocks in Oceanic Environments and Continental Ophiolite Complexes." American Journal of Science **273**(3): 207-239.

Wronkiewicz, D. J. and K. C. Condie (1987). "Geochemistry of Archean Shales from the Witwatersrand Supergroup, South-Africa - Source-Area Weathering and Provenance." Geochimica Et Cosmochimica Acta **51**(9): 2401-2416.

Wu, Y., S. Gao, H. Zhang, J. Zheng, X. Liu, H. Wang, H. Gong, L. Zhou and H. Yuan (2012). “Geochemistry and zircon U–Pb geochronology of Paleoproterozoic arc related granitoid in the Northwestern Yangtze Block and its geological implications.” Precambrian Research **200-203:** 26-37.

Yakymchuk, C., C. L. Kirkland and C. Clark (2018). "Th/U ratios in metamorphic zircon." Journal of Metamorphic Geology **36**(6): 715-737.

Zandt, G., et al. (2004). "Active foundering of a continental arc root beneath the southern Sierra Nevada in California." Nature **431**(7004): 41-46.

Figure 1

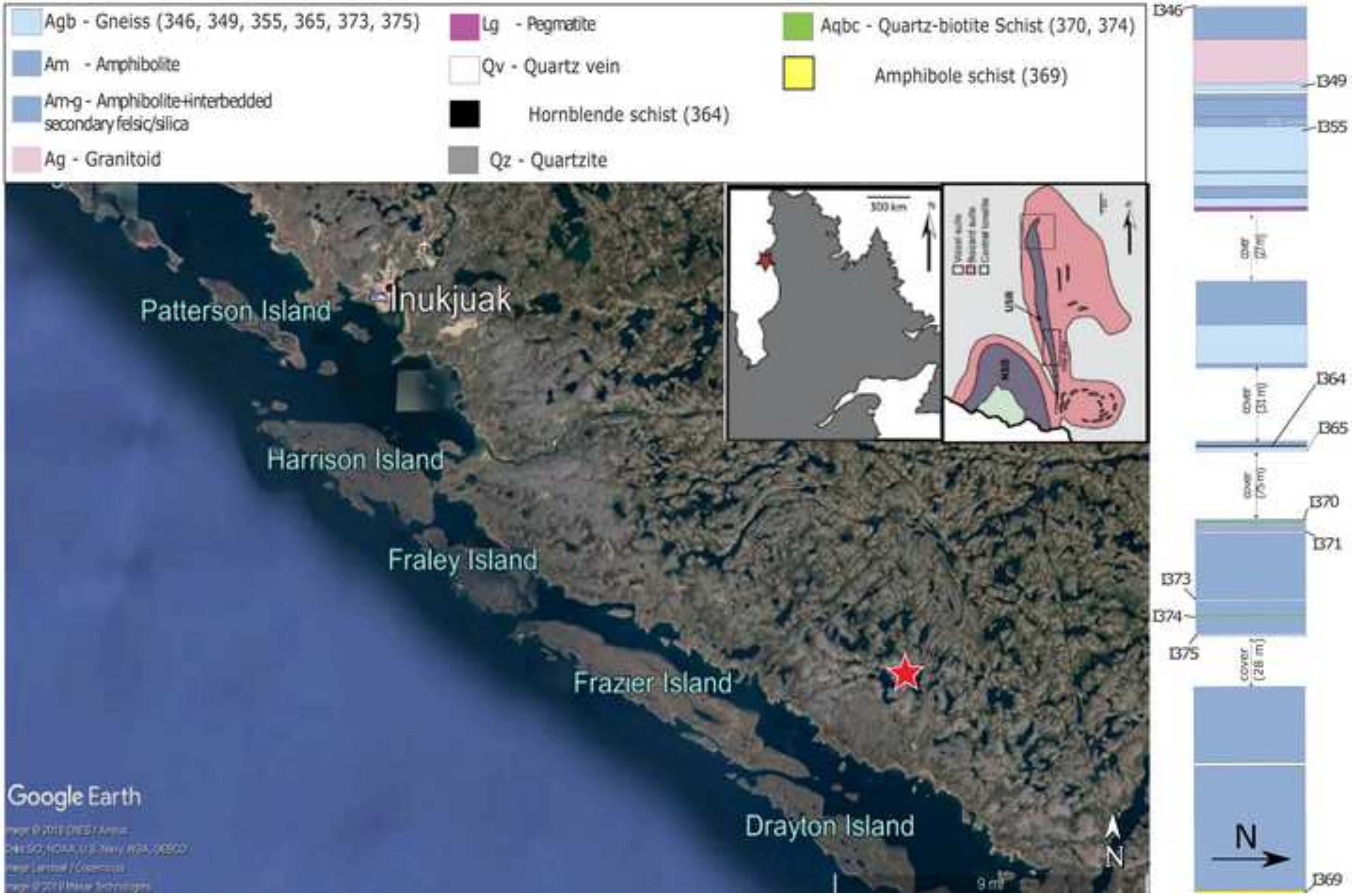
Agb - Gneiss (346, 349, 355, 365, 373, 375)
Am - Amphibolite
Am-g - Amphibolite+interbedded secondary felsic/silica
Ag - Granitoid
Lg - Pegmatite
Qv - Quartz vein
Hornblende schist (364)
Qz - Quartzite
Aqbc - Quartz-biotite Schist (370, 374)
Amphibole schist (369)
Patterson Island
Inukjuak
Harrison Island
Fraley Island
Frazier Island
Drayton Island
Google Earth
9 mi
N
300 km
USB
NSB
I346
I349
I355
cover (27 m)
cover (31 m)
I364
I365
cover (75 m)
I370
I371
I373
I374
I375
cover (28 m)
N
I369

Figure 2

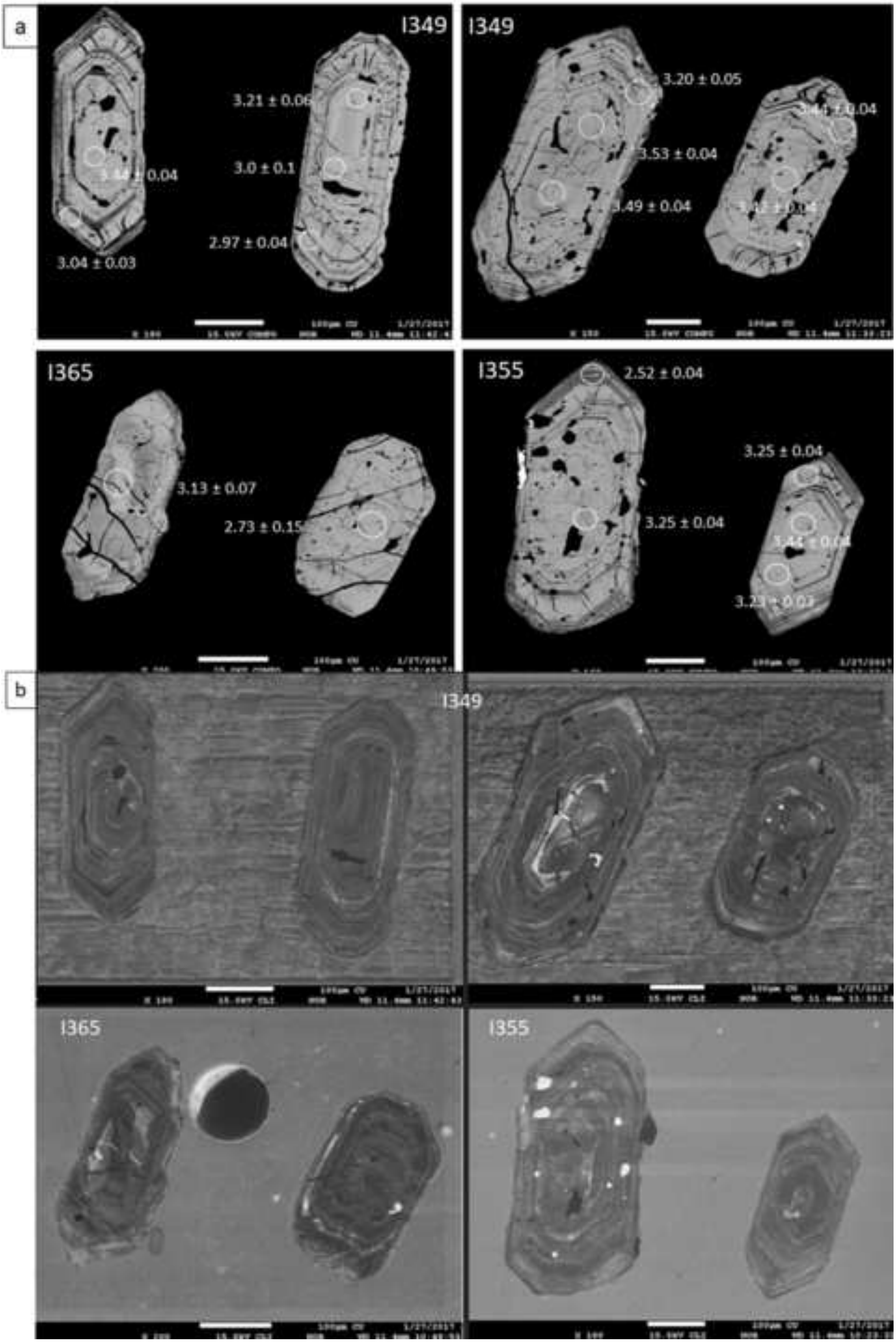

a
1349
3.44 ± 0.04
3.04 ± 0.03
3.21 ± 0.06
3.0 ± 0.1
2.97 ± 0.04
1349
3.20 ± 0.05
3.53 ± 0.04
3.49 ± 0.04
3.44 ± 0.04
1365
3.13 ± 0.07
2.73 ± 0.15
1355
2.52 ± 0.04
3.25 ± 0.04
3.25 ± 0.04
3.44 ± 0.04
3.23 ± 0.03
b
1349
1365
1355

Figure 3

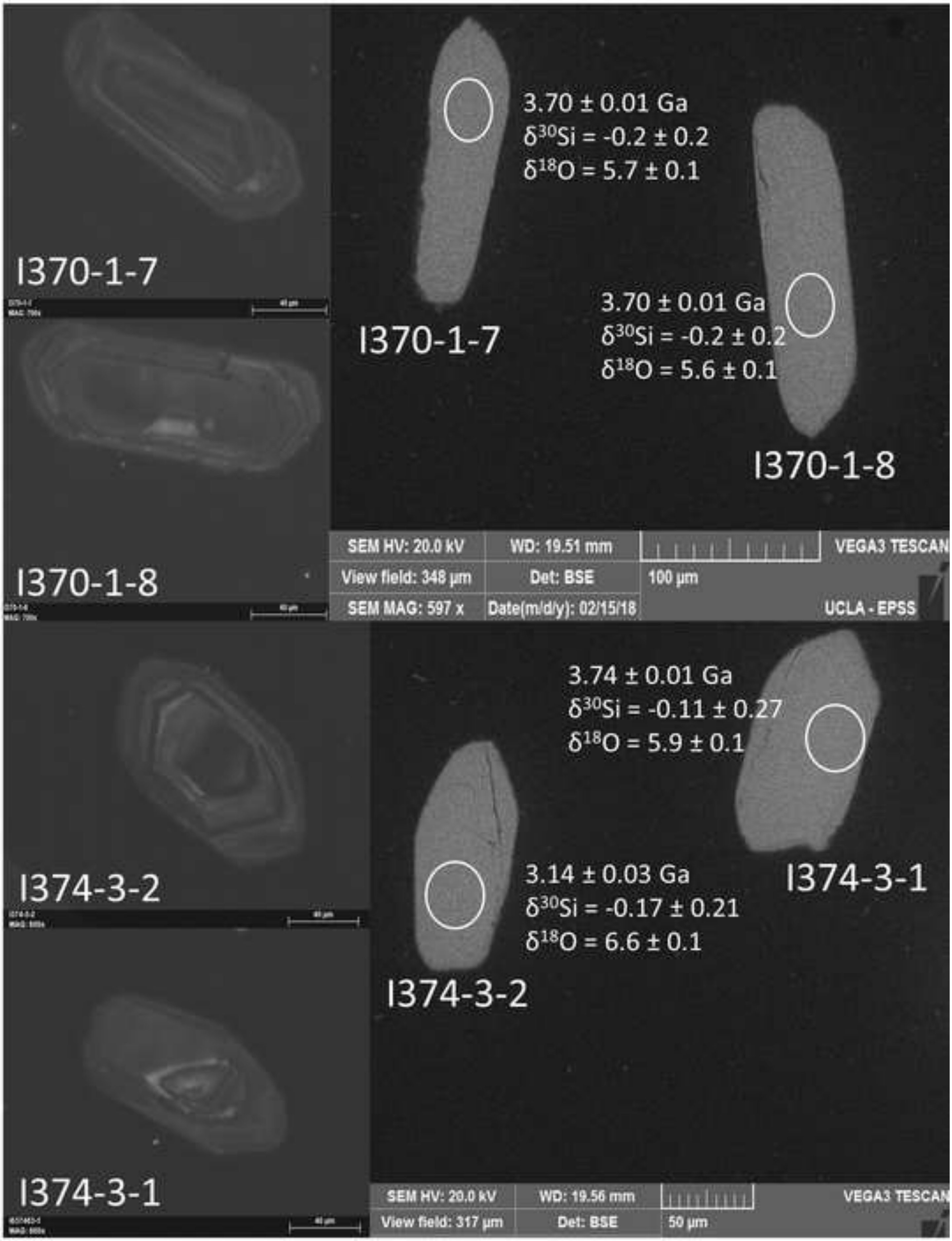
I370-1-7
I370-1-8
3.70 ± 0.01 Ga
δ30Si = -0.2 ± 0.2
δ18O = 5.7 ± 0.1
I370-1-7
3.70 ± 0.01 Ga
δ30Si = -0.2 ± 0.2
δ18O = 5.6 ± 0.1
I370-1-8
SEM HV: 20.0 kV
WD: 19.51 mm
VEGA3 TESCAN
View field: 348 µm
Det: BSE
100 µm
SEM MAG: 597 x
Date(m/d/y): 02/15/18
UCLA - EPSS
I374-3-2
I374-3-1
3.74 ± 0.01 Ga
δ30Si = -0.11 ± 0.27
δ18O = 5.9 ± 0.1
3.14 ± 0.03 Ga
δ30Si = -0.17 ± 0.21
δ18O = 6.6 ± 0.1
I374-3-2
I374-3-1
SEM HV: 20.0 kV
WD: 19.56 mm
VEGA3 TESCAN
View field: 317 µm
Det: BSE
50 µm

Figure 4

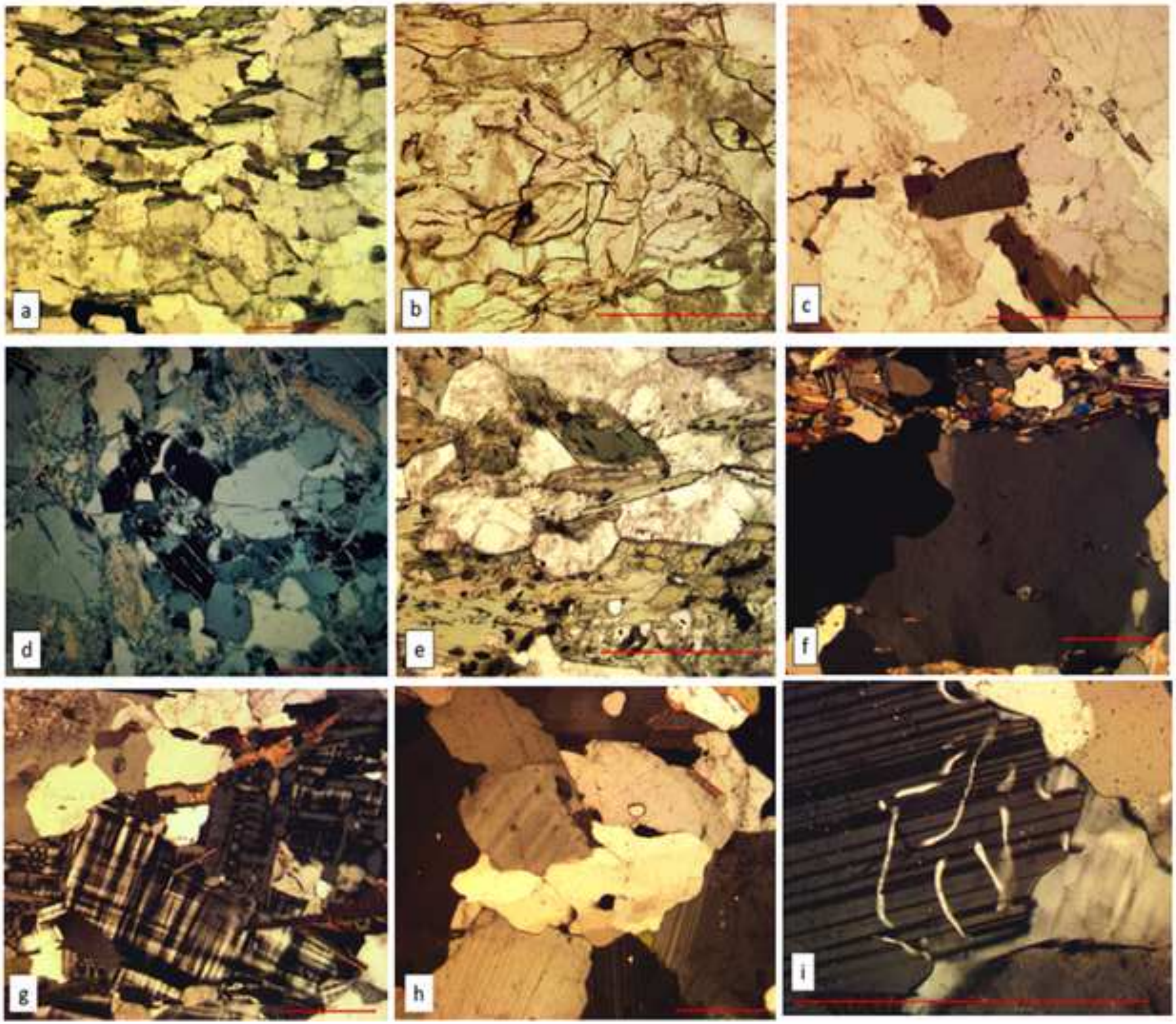

Figure 5

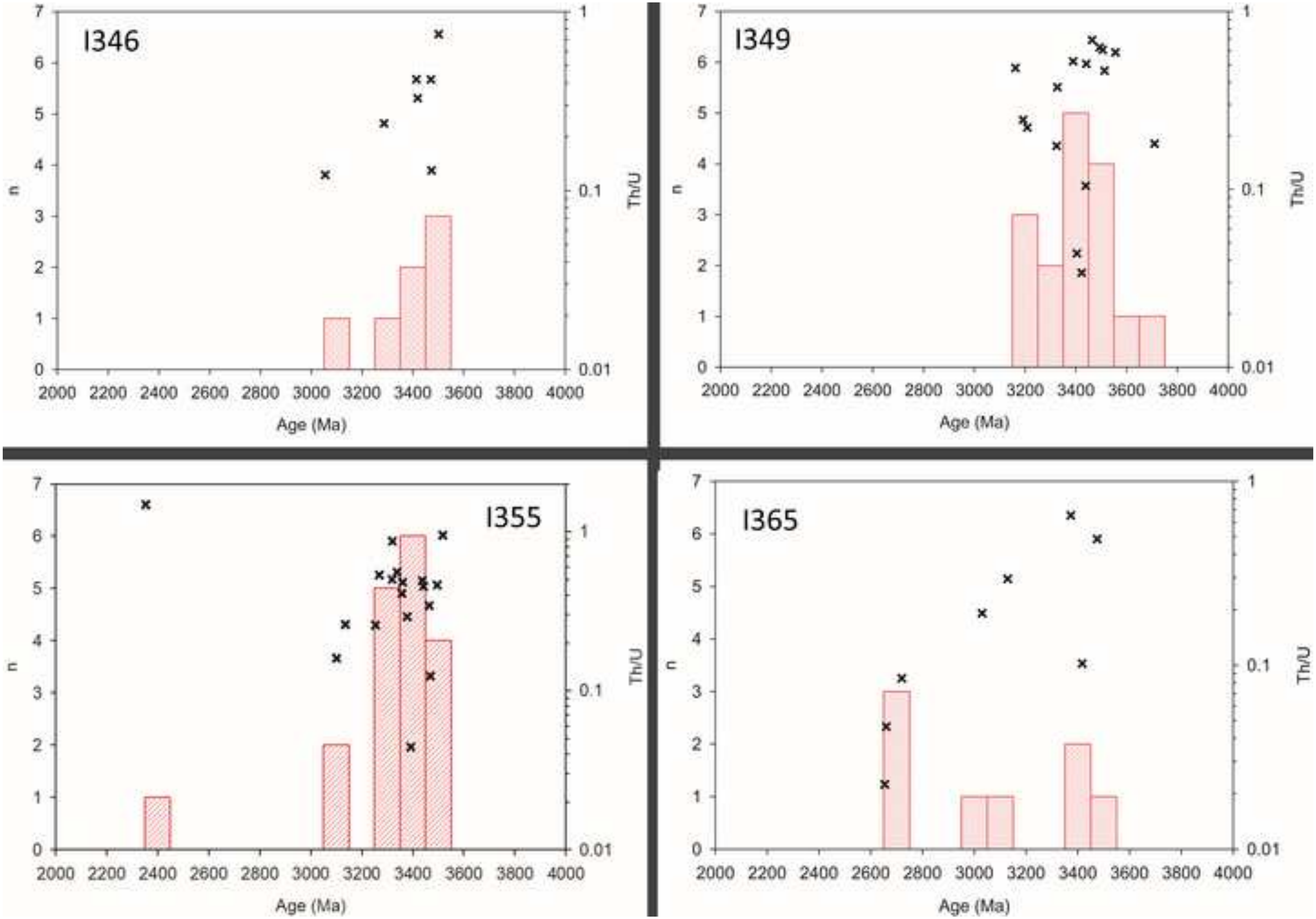
I346
I349
I355
I365
n
Th/U
Age (Ma)
0
1
2
3
4
5
6
7
0.01
0.1
1
2000
2200
2400
2600
2800
3000
3200
3400
3600
3800
4000

Figure 6

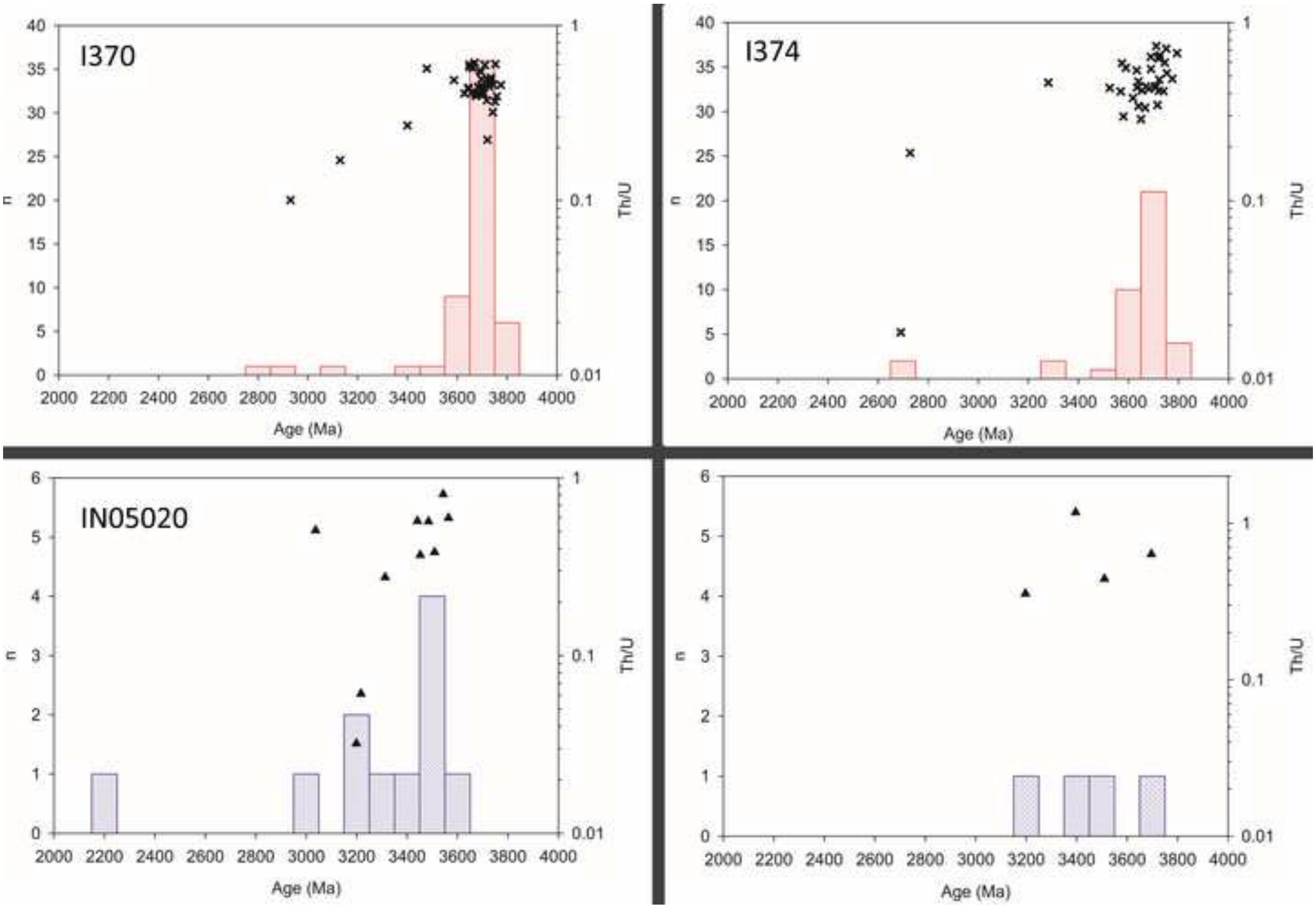
I370
I374
IN05020
n
Th/U
Age (Ma)
0
5
10
15
20
25
30
35
40
0.01
0.1
1
0
1
2
3
4
5
6
2000
2200
2400
2600
2800
3000
3200
3400
3600
3800
4000

Figure 7

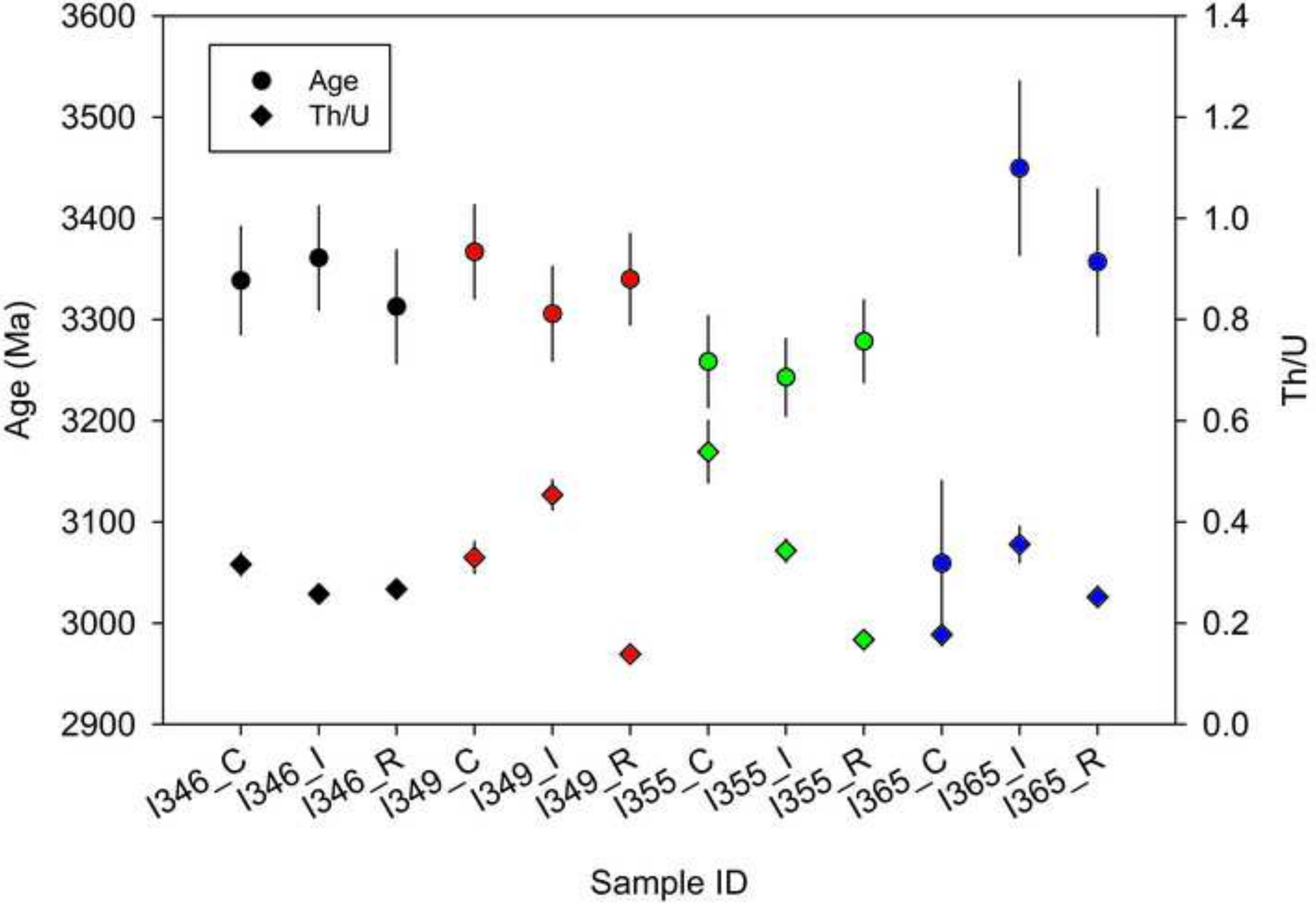

Age
Th/U
Age (Ma)
Th/U
Sample ID
3600
3500
3400
3300
3200
3100
3000
2900
1.4
1.2
1.0
0.8
0.6
0.4
0.2
0.0
I346_C
I346_I
I346_R
I349_C
I349_I
I349_R
I355_C
I355_I
I355_R
I365_C
I365_I
I365_R

Figure 8

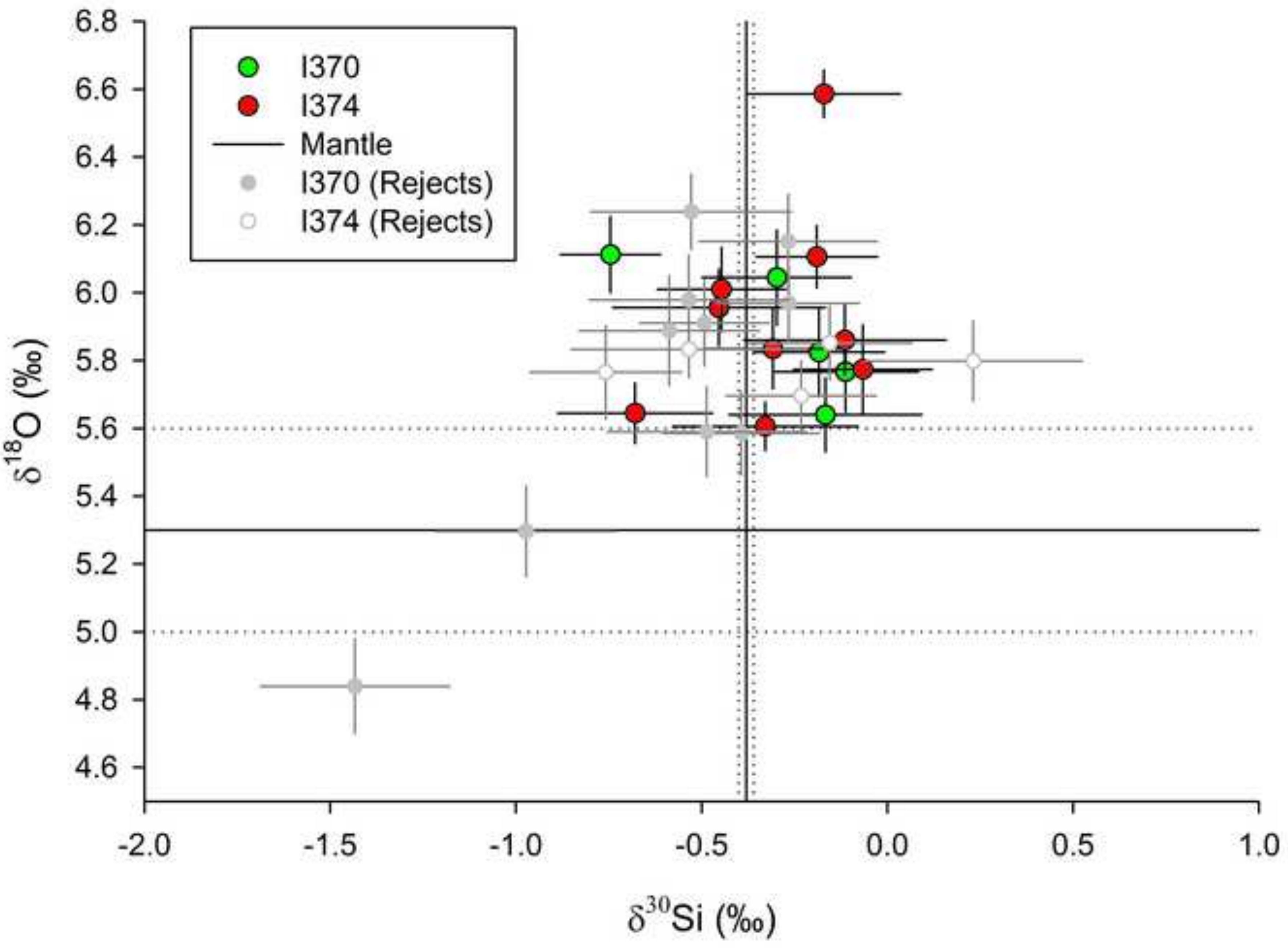
I370
I374
Mantle
I370 (Rejects)
I374 (Rejects)
6.8
6.6
6.4
6.2
6.0
5.8
5.6
5.4
5.2
5.0
4.8
4.6
δ18O (‰)
-2.0
-1.5
-1.0
-0.5
0.0
0.5
1.0
δ30Si (‰)

Figure 9

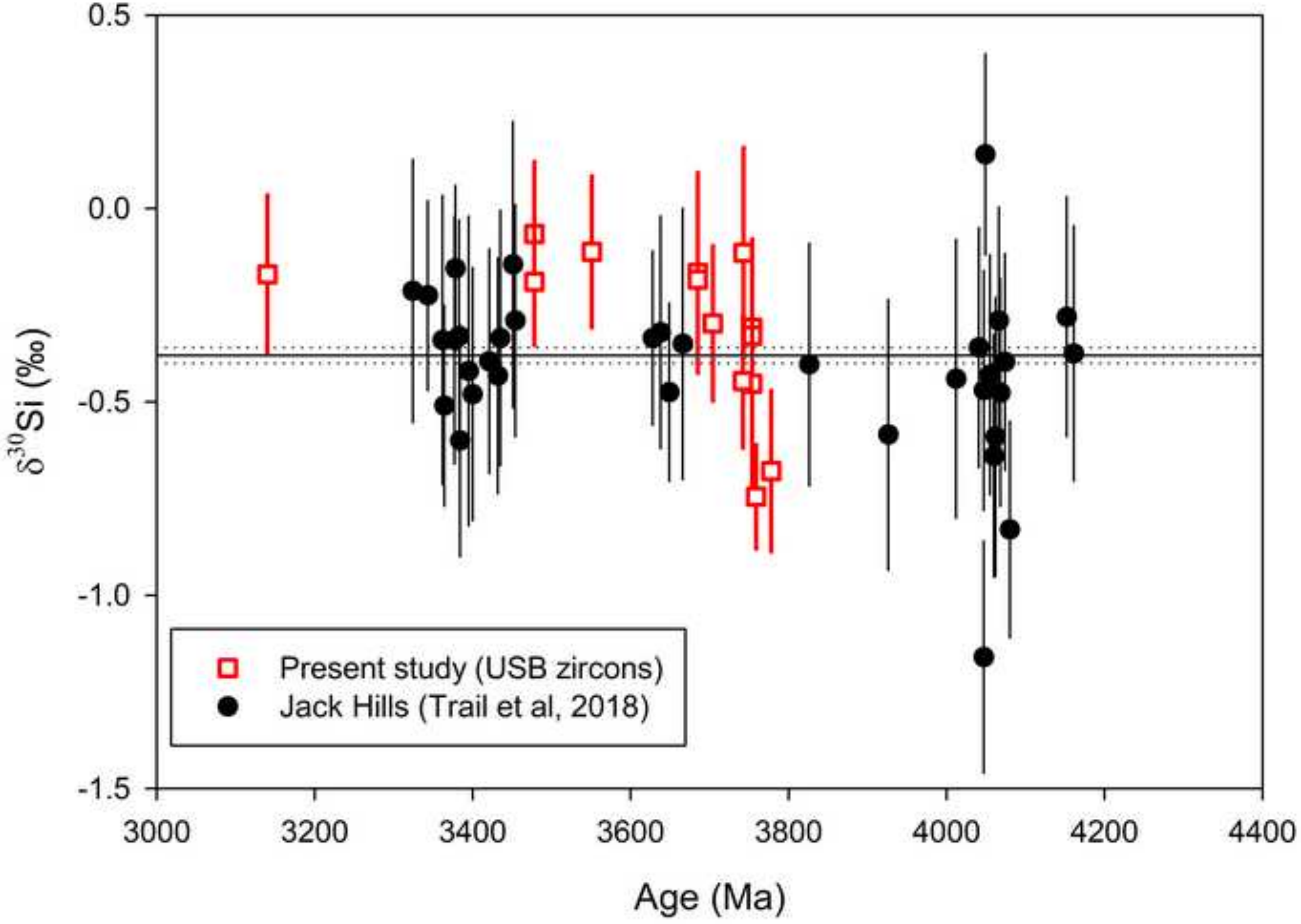
0.5
0.0
-0.5
-1.0
-1.5
δ^{30}Si (‰)
3000
3200
3400
3600
3800
4000
4200
4400
Age (Ma)
□ Present study (USB zircons)
● Jack Hills (Trail et al, 2018)

Figure 10

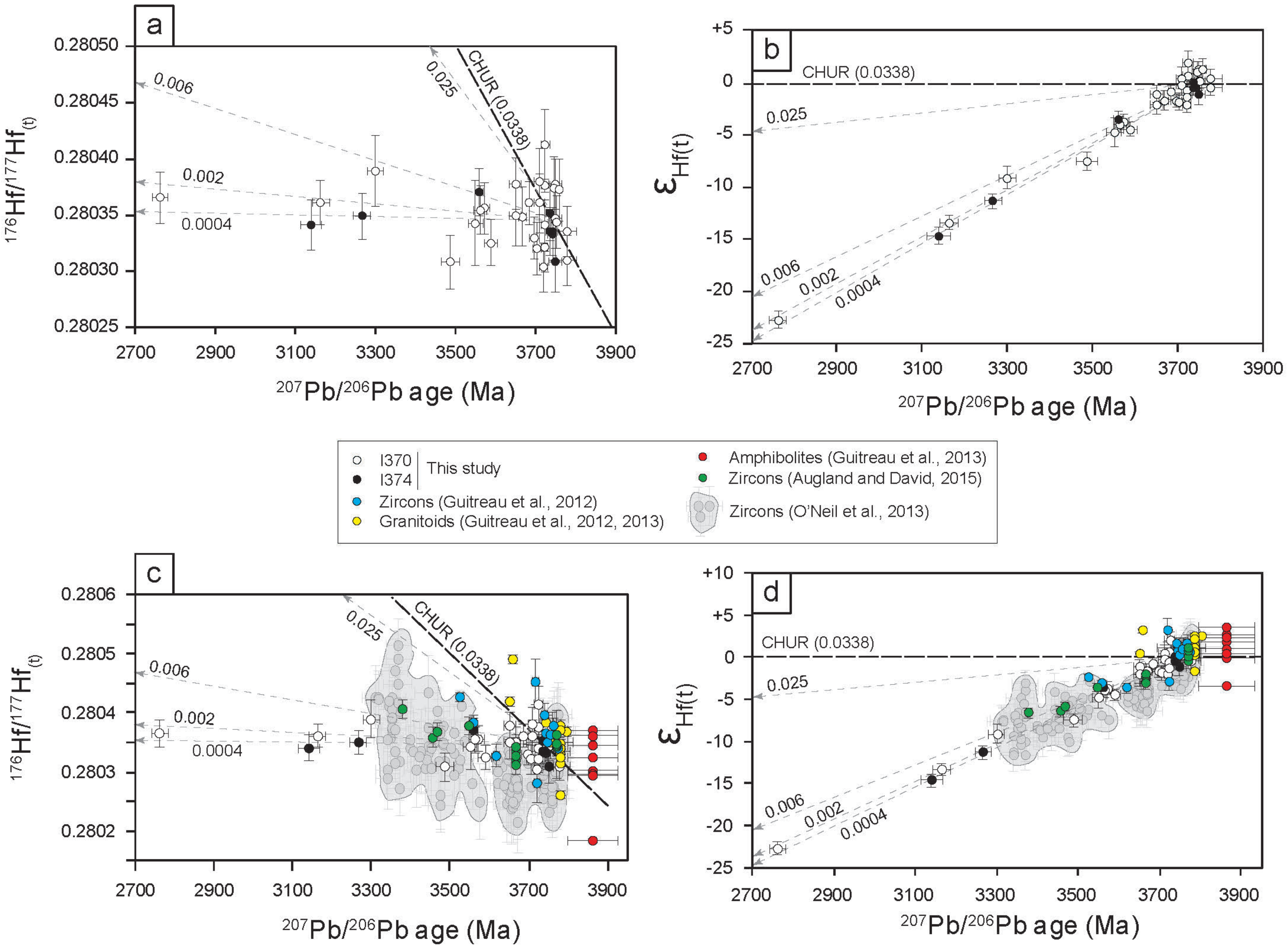
a
0.28050
0.28045
0.28040
0.28035
0.28030
0.28025
^{176}Hf/^{177}Hf$_{(t)}$
0.006
0.002
0.0004
0.025
CHUR (0.0338)
2700
2900
3100
3300
3500
3700
3900
^{207}Pb/^{206}Pb age (Ma)
b
+5
0
-5
-10
-15
-20
-25
ε$_{Hf(t)}$
CHUR (0.0338)
0.025
0.006
0.002
0.0004
I370
I374
This study
Zircons (Guitreau et al., 2012)
Granitoids (Guitreau et al., 2012, 2013)
Amphibolites (Guitreau et al., 2013)
Zircons (Augland and David, 2015)
Zircons (O'Neil et al., 2013)
c
0.2806
0.2805
0.2804
0.2803
0.2802
d
+10
+5
0
-5
-10
-15
-20
-25

Figure 11

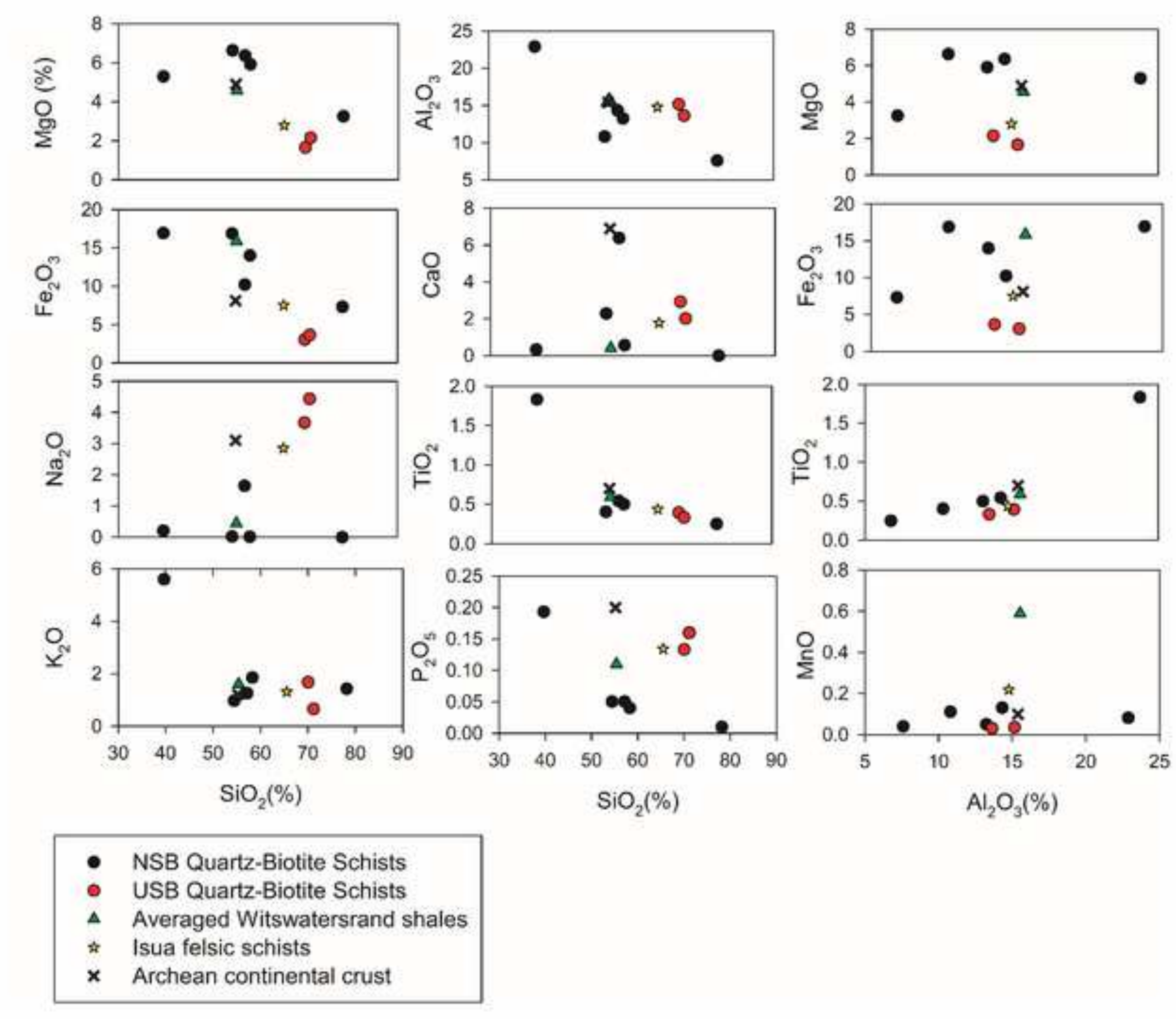
MgO (%)
Al_2O_3
MgO
Fe_2O_3
CaO
Fe_2O_3
Na_2O
TiO_2
TiO_2
K_2O
P_2O_5
MnO
SiO_2(%)
SiO_2(%)
Al_2O_3(%)
30 40 50 60 70 80 90
5 10 15 20 25
0 2 4 6 8
5 10 15 20 25
0 5 10 15 20
0 1 2 3 4 5
0.0 0.5 1.0 1.5 2.0
0 2 4 6
0.00 0.05 0.10 0.15 0.20 0.25
0.0 0.2 0.4 0.6 0.8
● NSB Quartz-Biotite Schists
● USB Quartz-Biotite Schists
▲ Averaged Witswatersrand shales
☆ Isua felsic schists
✕ Archean continental crust

Figure 12

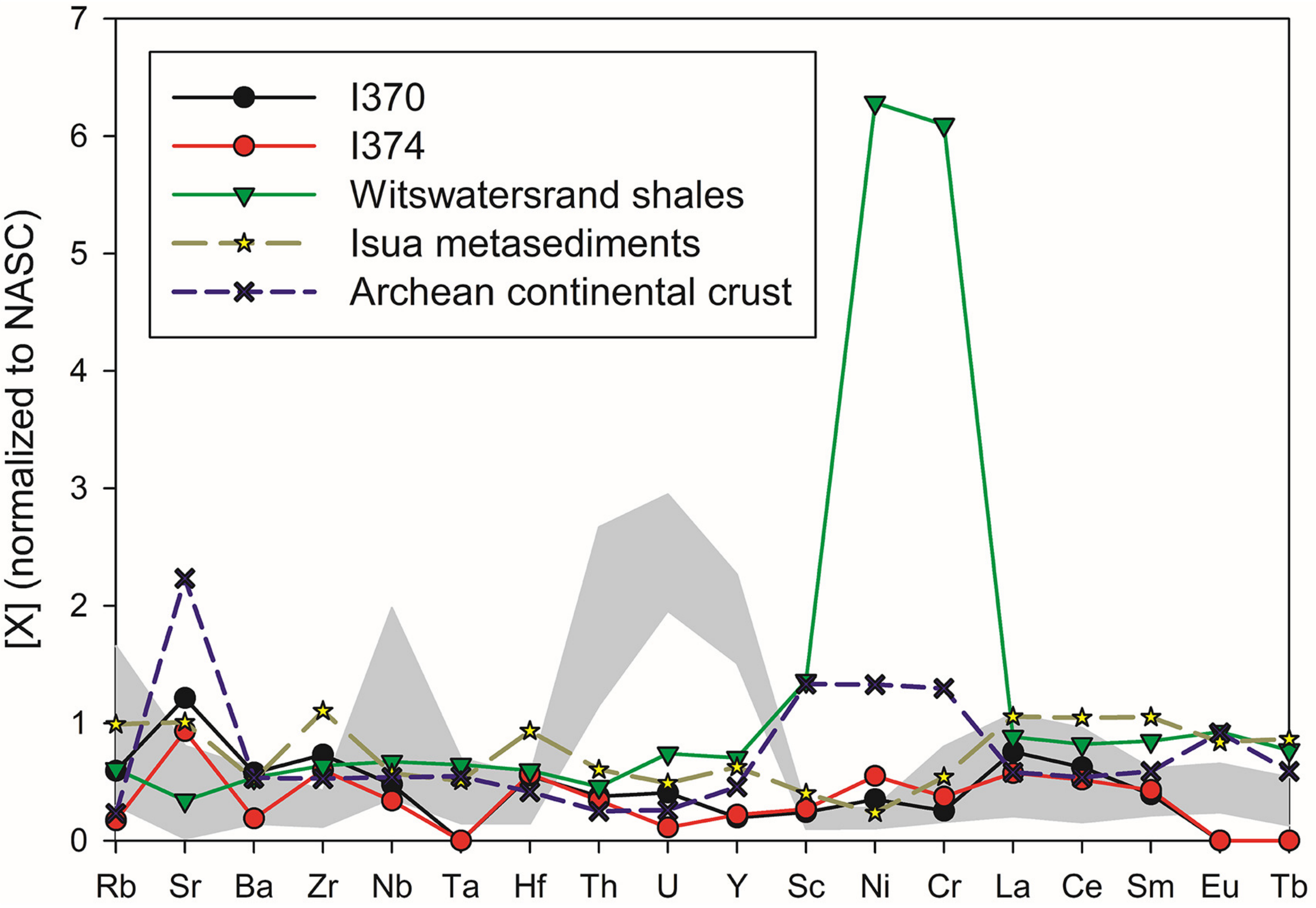
[X] (normalized to NASC)
7
6
5
4
3
2
1
0
I370
I374
Witswatersrand shales
Isua metasediments
Archean continental crust
Rb
Sr
Ba
Zr
Nb
Ta
Hf
Th
U
Y
Sc
Ni
Cr
La
Ce
Sm
Eu
Tb

Figure 13

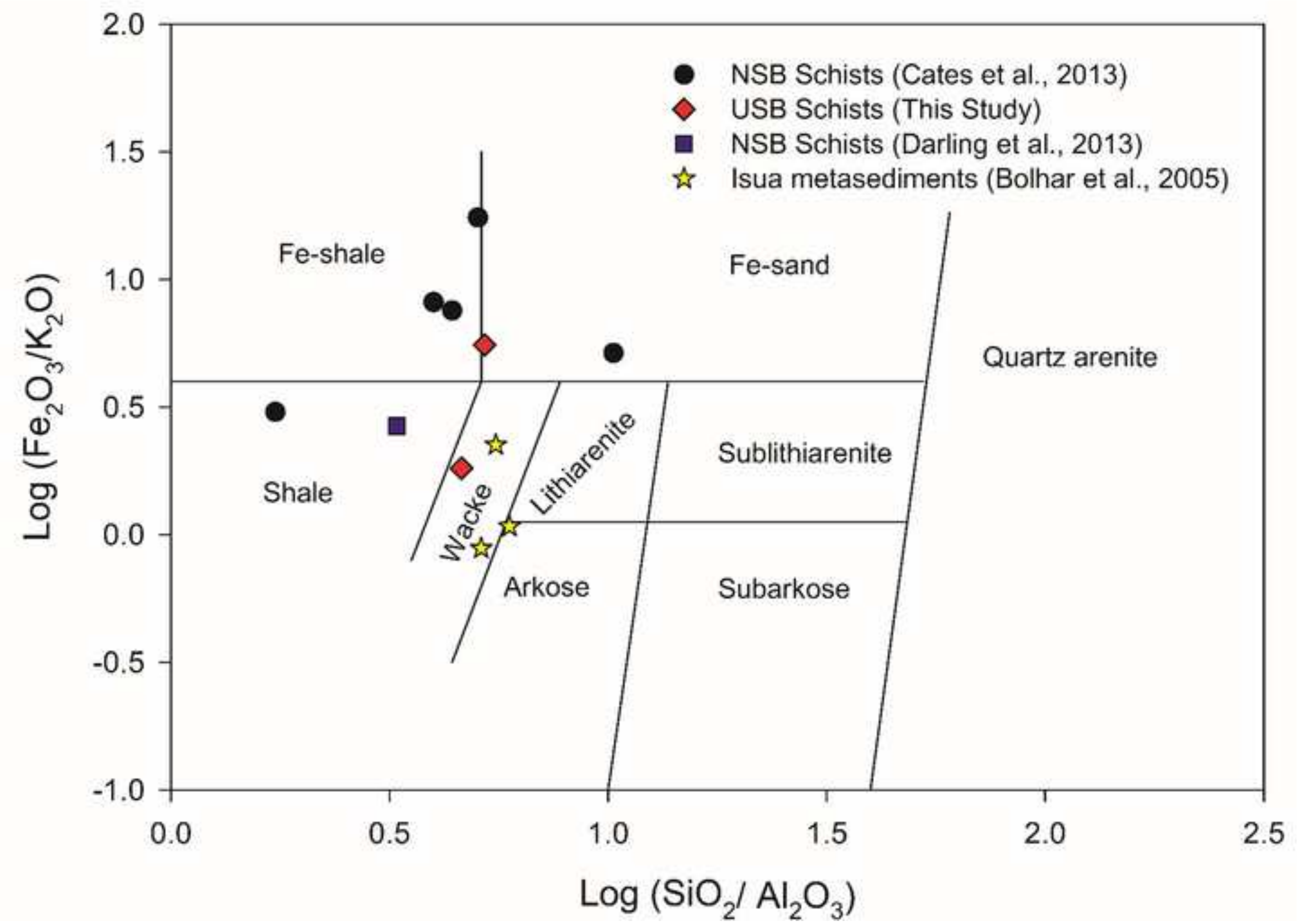

NSB Schists (Cates et al., 2013)
USB Schists (This Study)
NSB Schists (Darling et al., 2013)
Isua metasediments (Bolhar et al., 2005)
Fe-shale
Fe-sand
Quartz arenite
Lithiarenite
Sublithiarenite
Shale
Wacke
Arkose
Subarkose
2.0
1.5
1.0
0.5
0.0
-0.5
-1.0
0.0
0.5
1.0
1.5
2.0
2.5
Log (Fe_2O_3/K_2O)
Log (SiO_2/ Al_2O_3)

Table 1

Sample ID	Sample type	GPS Location	
		Latitude	Longitude
I239	Fuchsite-bearing Quartzite	58.27907°	-77.73080°
I240	Fuchsite-bearing Quartzite	58.27897°	-77.73091°
I346	Tonalitic orthogneiss	58.318044°	-77.692306°
I349	Granitic Orthogneiss	58.317987°	-77.692536°
I355	Tonalitic Gneiss	58.318018°	-77.692669°
I364	Hornblende Schist	58.317633°	-77.694142°
I365	Granitic Gneiss	58.317739°	-77.693695°
I369	Cummingtonite Schist	58.317037°	-77.693334°
I370	Quartz-Biotite Schist	58.317055°	-77.693349°
I373	Tonalitic Gneiss	58.316982°	-77.693538°
I374	Quartz-Biotite Schist	58.316985°	-77.693595°
I226	Unconsolidated Sediment	58.285324°	-77.697742°
I235	Unconsolidated Sediment	58.275978°	-77.684671°
I247	Unconsolidated Sediment	58.282120°	-77.728605°
I300	Unconsolidated Sediment	58.300750°	-77.688830°

Table 2

Sample ID	U-Pb Age(Ga)				Th/U
	LA-ICPMS (Average)	LA-ICPMS (Oldest)	SIMS (Average)	SIMS (Oldest)	
I239	-		-	-	-
I240	-		-	-	-
I295	-		-	-	-
I346	3.34 ± 0.05	3.50 ± 0.05	-	-	0.32 ± 0.02
I349	3.37 ± 0.05	3.49 ± 0.04	-	-	0.33 ± 0.03
I355	3.26 ± 0.05	3.52 ± 0.04	-	-	0.54 ± 0.06
I364	-		-	-	-
I365	3.31 ± 0.09	3.47 ± 0.08	-	-	0.26 ± 0.03
I369	-		-	-	-
I370	3.66 ± 0.06	3.78 ± 0.08	3.68 ± 0.01	3.76 ± 0.01	0.44 ± 0.06
I373	3.66 ± 0.06	3.68 ± 0.07	-	-	0.60 ± 0.05
I374	3.68 ±0.07	3.79 ± 0.04	3.67 ± 0.01	3.75 ± 0.01	0.52 ± 0.07
I375	-		-	-	-
I226	2.68 ± 0.12	3.49 ± 0.12	-	-	0.69 ± 0.13
I235	2.77 ± 0.08	3.56 ± 0.06	-	-	0.75 ± 0.12
I247	2.57 ± 0.08	3.21 ± 0.08	-	-	0.26 ± 0.04
I300	2.74 ± 0.08	3.45 ± 0.05	-	-	0.64 ± 0.09